Hydraulic conductivity distribution in crystalline rocks, derived from inflows to tunnels and galleries in the Central Alps, Switzerland

Journal Article

Author(s):
Masset, Olivier; Loew, Simon (iD)

Hydraulic conductivity distribution in crystalline rocks, derived from inflows to tunnels and galleries in the Central Alps, Switzerland

Olivier Masset · Simon Loew

Abstract Inflow data from 23 tunnels and galleries, 136km in length and located in the Aar and Gotthard massifs of the Swiss Alps, have been analyzed with the objective (1) to understand the 3-dimensional spatial distribution of groundwater flow in crystalline basement rocks, (2) to assess the dependency of tunnel inflow rate on depth, tectonic overprint, and lithology, and (3) to derive the distribution of fracture transmissivity and effective hydraulic conductivity at the 100-m scale. Brittle tectonic overprint is shown to be the principal parameter regulating inflow rate and dominates over depth and lithology. The highest early time inflow rate is 1,300l/s and has been reported from a shallow hydropower gallery intersecting a 200-m wide cataclastic fault zone. The derived lognormal transmissivity distribution is based on 1,361 tunnel intervals with a length of 100m. Such interval transmissivities range between 10^{-9} and 10^{-1}m^2/s within the first 200–400m of depth and between 10^{-9} and 10^{-4}m^2/s in the depth interval of 400–1,500m below ground surface. Outside brittle fault zones, a trend of decreasing transmissivity/hydraulic conductivity with increasing depth is observed for some schistous and gneissic geological units, whereas no trend is identified for the granitic units.

Keywords Hydraulic properties · Crystalline rocks · Fractured rocks · Tunnel · Switzerland

Introduction

Tunnel inflows

Several researchers have focused on tunnel inflow phenomena. Among the different aspects of the phenomena considered are the inflow distribution, the inflow rate transient behavior and the source of inflows. One of the most popular study approaches, whatever the aspect considered, is the comparison of measured inflow data with modeled inflows in order to back calculate hydrogeological parameters. For example, Zhang and Franklin (1993) compiled inflow data from different tunnels in different types of rock and compared them with analytical and numerical models, and Hwang and Lu (2007) modeled inflow transient behavior and found it to be in agreement with the general trend of measured inflow data.

The analysis of tunnel inflow data yields important information about the spatial distribution of groundwater flow at various scales and the hydraulic properties of rock masses. Deriving large-scale hydrogeological properties of crystalline rocks is of relevance for the site selection of waste repositories, for geothermal and hydrocarbon reservoir exploitation, for groundwater resource management, and for tunneling. Standard borehole tests carried out from the ground surface only yield local hydraulic properties. In comparison, the rock mass volume affected by the pressure disturbance caused by a deep underground excavation is larger. This is due to the strong pressure drawdown caused by a deep draining tunnel, the large tunnel diameter, and the long drainage duration. This implies that the analysis of tunnel inflows provides estimates of hydraulic properties relevant for a large-scale investigation. In addition to this large-scale investigation, tunnels are often relatively long "sampling lines". In the case of detailed geological and hydrogeological tunnel observations, not only major inflows from faults and fault zones but also minor inflows from the fractured rock mass can be studied. This implies that tunnel observations can also lead to multi-scale information about flow in fractured rocks (Masset and Loew 2007).

Back analyses of tunnel inflows rely on the same principles and models like forward predictions of tunnel inflows. Several simple mathematical models have been published that can explain or predict the temporal behavior of groundwater inflows to tunnels in rocks assuming homogeneous hydraulic conductivities and a Darcy type of groundwater flow. Most of these models assume two-dimensional (2D) flow in a plane perpendicular to the tunnel axis and a constant head boundary condition at the tunnel wall, which is often assumed to have a circular geometry. For a deep tunnel (tunnel radius $r \ll$ depth of tunnel below water table) in a homogeneous

O. Masset (✉) · S. Loew
Geologisches Institut, NO G 69.1,
Sonneggstrasse 5, 8092, Zurich, Switzerland
e-mail: olivier.masset@erdw.ethz.ch
Tel.: +41-44-6332737
Fax: +41-44-6331108

rock mass with a linear constant pressure boundary at the surface (for example a lake or a prolific aquifer), the steady state inflow rate Q into a tunnel segment of length L can be described by the well known formula reported by Goodman et al. (1965):

$$Q = \frac{2\pi K L (h_e - h_t)}{2.3 \log(2(h_e - h_t)/r)} \qquad (1)$$

where K [m/s] is the effective hydraulic conductivity (or equivalent porous medium hydraulic conductivity) in the (vertical) plane of flow, $h_e - h_t$ [m] is the tunnel drawdown (i.e. the difference between the static formation head and the tunnel head), and r [m] is the tunnel radius (see Appendix 1). Lei (1999, 2000) derived an analytical solution for the steady-state head field and groundwater flow around a tunnel close to the surface. Zhang and Franklin (1993) proposed another analytical solution to model an assumed exponential decrease of the hydraulic conductivity with depth. El Tani (1999) gives approximate solutions for steady-state inflow to tunnels with elliptical or square cross-sections.

Flow in fractured rocks

According to many authors such as Zhao (1998), groundwater flow in crystalline rock masses is controlled by flow in discontinuities such as faults and fractures. The prediction of inflows to tunnels in fractured crystalline rocks is a difficult task, because the permeability distribution of fractured crystalline rocks is strongly heterogeneous and ranges over several orders of magnitude. In addition, only a few highly conductive pathways control the total groundwater flow on different scales in the rock mass surrounding a deep tunnel (Loew 2001; Long et al. 1991). In the past, several researchers have attempted to model heterogeneous flow in fractured rock masses with discrete fracture network models (Cacas et al. 1990; Davy et al. 2006; Wang et al. 2001). This approach assumes that the fracture network geometry is known or can be rebuilt from borehole fracture data or surface-fracture trace maps. In such cases, the transmissivity distribution of the fracture sets that form a conductive network can be obtained by back analysis of distributed tunnel inflow data (Molinero et al. 2002).

Most of the time, the fractures are assumed to have a constant hydraulic aperture and, thus, a constant transmissivity. This is of course a simplification, because field observations suggest that faults or large joints have complex internal geometries. An alternative is to assign each fracture a transmissivity distribution instead of a constant transmissivity value (Mourzenko et al. 1996, 1999). In that case, the transmissivity distribution is derived from the geometric fracture aperture distribution. Unfortunately, no data concerning fracture aperture distribution are available for real cases at site scales. Moreover, faults are, most of the time, filled with crushed material and their width may vary drastically, even at the

scale of a tunnel diameter, which renders the transmissivity distribution within a fault difficult to assess.

Study motivation and objectives

Since the construction of the Gotthard railway tunnel in the years 1872–1880, numerous underground excavations have been constructed in the crystalline basement rocks of the Aar and Gotthard massifs of the central Swiss Alps. These underground excavations include several train and road tunnels for N–S and W–E connections through the Swiss Alps, numerous hydropower drifts and galleries, and some military installations. The geological findings of most of these underground constructions are described in unpublished technical reports; only a few observations are published (Keller and Schneider 1982; Keller et al. 1987; Klemenz 1974). A reference list of the unpublished reports can be found in Table 1. The unpublished reports include the locations and rates of groundwater inflows, geological cross-sections including lithology, tectonic unit, major fractures and faults, and other geotechnical properties. While most military reports are still confidential, a great number of unpublished reports dealing with traffic and hydropower constructions are available for scientific purposes. The total length of the underground excavations which have accessible documentation is 136 km. A first attempt to quantitatively analyze these observations has been made for the design of the Gotthard base tunnel (Loew et al. 2000; Löw et al. 1996). This study presents a complete description of this unique data set and an analysis of the following hydrogeological key properties of fractured crystalline rocks in the Aar and Gotthard massifs:

– Distribution of inflow frequency and rate as a function of depth and lithology
– Spacing distribution of different types of tunnel inflows
– Impact of brittle faulting and fracturing on tunnel inflows
– Regional variability of preferential groundwater pathways and controlling parameters
– Estimate of the distribution of fracture transmissivity
– Estimate of the distribution of rock mass effective hydraulic conductivity

Location and geological setting of the study area

The study area is located in the central Aar and Gotthard massifs of the Swiss Alps (Figs. 1 and 2). There are distinct tectonic, lithologic and metamorphic differences between the Aar and Gotthard massifs, which are explained in the following.

Ground elevation in the central Aar massif ranges from 475 m (Erstfeld) to 3,085 m (Piz Giuv) above mean sea level. The Aar massif is striking NE, is 115 km long, 23 km wide and covers an area of about 2,000 km^2. It is composed of pre-Variscan polyorogenic and polymetamorphic basement rocks (primarily gneisses, schists and migmatites) intruded by late Variscan magmatic rocks (granites, diorites,

Table 1 References to unpublished reports

Grundner (1942) Geologisch-petrographische Aufnahme der Zuleitung Haslital der Kraftwerk Oberhasli AG [Geological and petrological survey of the Haslital adit of the Oberhasli AG power plant] Stollenaufnahmen 1:1000, Pläne Kraftwerk Innertkirchen, Ablaufkanal, Zentrale, Wasserschloss, Benzlani, Hostet

Hügi T (1961) Zuleitung der Unteralpreuss in den Ritomsee-Zulaufstollen: Geologisches Längsprofil 1:2000/1:200 und Ausfuhrungsplan SBB [Diversion of the Unteralpreuss River to the Ritom Lake-gallery: geological longitudinal profile and Swiss Federal railway project plan]

Loew S, Masset O (2008) Groundwater resources in fractured aquifers of Switzerland: estimations derived from tunnel inflows and surface springs in the Gotthard massif (Switzerland). ETH Report No. 3465/62, ETH, Zurich, Switzerland

SBB Druckstollenkomission (1923) Bericht der Druckstollenkomission über den Druckstollen des Kraftwerks Amsteg [Report of the Pressure Tunnel commission on the pressure tunnel of the Amsteg power plant]. Lage der Versuchsstrecken im Zulaufstollen mit geologischer Diagnose nach Prof Dr Hugi Uebersichtslängenprofil und Lageplan 1:10000/1000 und 1:10000, SBB

Schneider TR (1972) Gotthard Basistunnel: Petrographische Sammelprofile durch das Tavetscher Zwischenmassiv und Gotthardmassiv 1:5000 aufgrund der Aufnahmen in den Stollen der Wasser Kraftwerke Vorderrhein [Gotthard base tunnel: petrological profile through the Tavetsch and Gotthard massifs 1:5000 based on the survey of the Vorderrhein hydropower plant galleries]. zusammengestellt von Dal Vesco E. Auswertung der Stollenaufnahmen NOK, Wasseranfall im Horizontalschnitt 1:25000 Unveröffentlicher Bericht 307e/3,5

Schneider TR (1979) Gotthard Strassentunnel: Geologischer Schlussbericht Nordseite IV Bergwasserführung Chemismus und Temperaturen, Geologisches Befundprofil durch Tunnelröhre 1:10000 [Gotthard highway tunnel: final geological report of the northern part number 4—groundwater flow, chemistry and temperatures, geological profile along the tunnel at the 1:10000 scale]. Unveröffentlicher Bericht 305am

Schneider TR (1985) Basis-Tunnel Furka - Geologischer Schlussbericht, Geologische Aufnahme 1:200 des Tunnels Los 62 Realp und Fensters Los 63 Bedretto [Furka base tunnel: final geological report, geological 1:200 scale map of the Realp and Bedretto legs]. Unveröffentlichte Berichte 338f, 338g, 338o

Stapff FM (1882) Geologische Aufnahme des Gotthard-Bahntunnels: 60 Geologische Tunnelprofile 1:200 (Längen- und Horizontalschnitte) [Geological survey of the Gotthard railway tunnel: 60 geological 1:200 scale vertical and horizontal profiles of the tunnel]. Quartalsberichte zu Handen des Schweizerischen Bundesrates, Geneva

Voborny O, Resele G, Vomvoris S (1993) Hydrogeology of crystalline rocks of northern Switzerland: synthesis of hydraulic borehole data and assessment of effective properties. Nagra Internal Report NIB 92-87, Nagra, Baden, Switzerland

Winterhalter RU (1949a) Kraftwerk Wassen: Geologischer Schlussbericht—Geologisches Profil längs des Druckstollens 1:5000 [Wassen power plant: final geological report—geological profile along the pressure gallery at the 1:5000 scale]. Unveröffentlicher Bericht 113b/2

Wanner H (1982) Galleria Stradale del San Gottardo, Rapporto Finale Lotto Sud: Profilo Idrogeologico attraverso il tunnel stradale del Gottardo 1:10000 [Gotthard highway tunnel, final report of the southern section: hydrogeological profile along the tunnel at the 1:10000 scale]

Winterhalter RU (1949b) Kraftwerk Lucendro: Geologischer Schlussbericht—Geologisches profil längs des Druckstollens 1:10000 [Lucendro power plant: final geological report—geological profile along the pressure gallery at the 1:10000 scale]. Unveröffentlichte Berichte 47e/3

Winterhalter RU (1957) Kraftwerk Ritom: Zuleitung der Garegna: Geologischer Schlussbericht, Geologische Stollenaufzeichnungen 1:500 [Ritom power plant: diversion of the Garegna River—final geological report, geological profile

of the gallery at the 1:500 scale]. Unveröffentlicher Bericht 109o/1

Winterhalter RU (1969a) Kraftwerk Göschenen: Geologischer Schlussbericht—Geologische Stollenaufnahme 1:1000 der Zuleitung der Furkareuss und der Zuleitung der Voralpreuss [Goeschenen power plant: final geological report—geological 1:1000 scale profile along the supply gallery from the Furkareuss and the Voralpreuss rivers]. Unveröffentlichte Berichte 122v/3-1,4 122v/4,1

Winterhalter RU (1969b) Kraftwerk Göschenen: Geologischer Schlussbericht—Herkunft der Gesteinproben und Wasseranfall 1:10000, geologisches Profil durch die Zuleitung Furkareuss 1:10000 [Goeschenen power plant: final geological report—origin of the rock samples and inflows at the 1:10000 scale, geological profile along the supply gallery of the Furkareuss River 1:10000]. Unveröffentlichte Berichte 122v/2-1,4-10

Winterhalter RU, Dal Vesco E (1961) Gotthardtunnel SBB, Vortrieb und Wasseranfall [Gotthard railway tunnel, excavation and inflows]. Unveröffentlicher Plan, 215a/6

syenites and in a smaller proportion volcanites, aplites and lamprophyres) and covered by Permian and Mesozoic sediments (Abrecht 1994; Labhart 1977).

During the Tertiary alpine collision, the Aar massif was strongly compressed and thrusted in the NW direction. In the north, the sedimentary cover was folded and thrusted onto the basement rocks, and finally the southern margin was turned in a nearly upright position (Schmid et al. 1996; Steck 1968a; Steck and Hunziker 1994). The Tertiary collision lead to an Alpine foliation and heterogeneous ductile deformations at all scales. The greenschist facies Alpine metamorphic overprint increases from NW to SE (Choukroune and Gapais 1983; Frey et al. 1980; Labhart 1977; Laws 2001; Meyer et al. 1989; Steck 1984). Presumably since the Miocene, ductile deformations have been superimposed by weak brittle deformations and a large-scale uplift in the order of 0.5–1.0 mm/year takes place (Kohl et al. 2000). This resulted in the formation of small shear fractures and joint systems (Laws et al. 2000). According to Laws (2001) and Frei and Löw (2001), steeply dipping ENE–WSW striking shear zones of the study area are primarily ductile but more fracture-bearing than the host rock. This is supported by recent observations in the Gotthard base tunnel (Frei and Breitenmoser 2006).
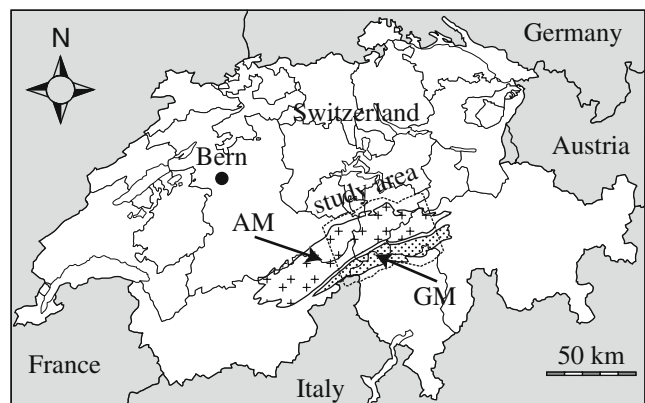

Fig. 1 Sketch of Switzerland showing the perimeter of the study area (*tilled line*) and the location of the Aar massif (*AM*) and Gotthard massif (*GM*)
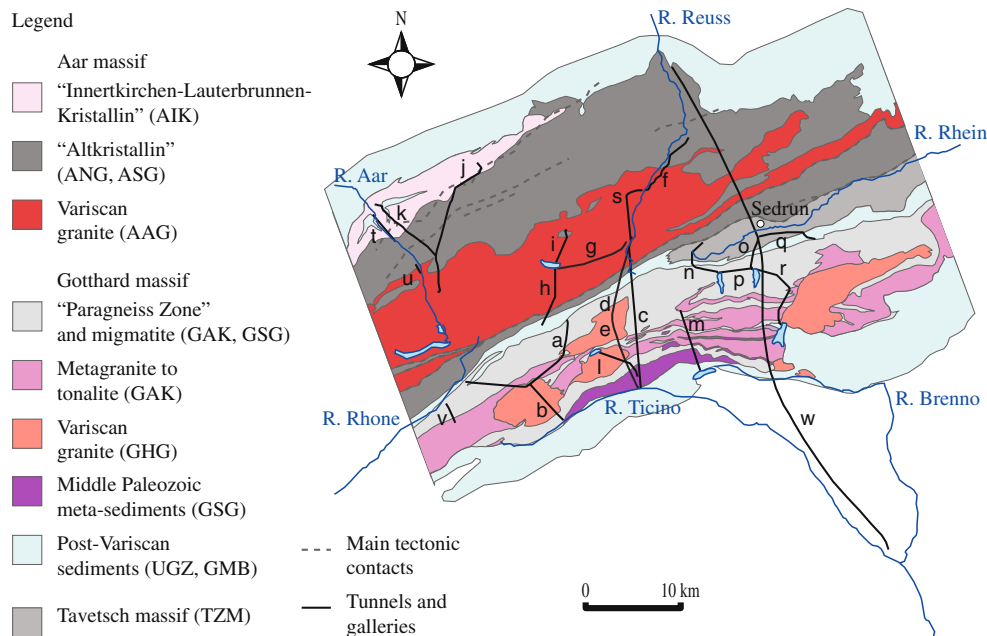
Fig. 2 Map of the study area showing the main rivers, the main lithologies (their corresponding geological units, modified from Labhart (1999), the main tectonic units and tectonic contacts with *black lines* representing: Furka base tunnel Realp leg (*a*); Furka base tunnel Bedretto window gallery (*b*); Gotthard SBB railway tunnel (*c*); Gotthard A2 highway security gallery (*d*); Gotthard A2 highway main tunnel (*e*); KW Amsteg supply gallery (*f*); KW Goeschenen pressure gallery (*g*); KW Goeschenen Furkareuss supply gallery (*h*); KW Goeschenen Voralpreuss supply gallery (*i*); KW Oberhasli Gadmenwasser supply gallery (*j*); KW Oberhasli Handegg supply gallery (*k*); KW Lucendro pressure gallery (*l*); KW Ritom Garegna and Unteralpreuss supply galleries (*m*); KW Vorderrhein Val Val-Curnera gallery (*n*); KW Vorderrhein Tgom-Nalps gallery (*o*); KW Vorderrhein Curnera-Nalps gallery (*p*); KW Vorderrhein Sedrun-Medels gallery (*q*); KW Vorderrhein Nalps-St Maria gallery (*r*); KW Wassen supply gallery (*s*); Gas Transit Urweid gallery (*t*); Gas Transit Gstelli gallery (*u*); Gas Transit Obergesteln gallery (*v*); Gotthard base tunnel (under construction) (*w*)

The Gotthard massif, which is also striking NE, is 80 km long and 12 km wide and covers an area of 580 km² (Fig. 2). Ground elevation ranges from 1,147 m (Andermatt) to 2,963 m (Pizzo Lucendro). The Gotthard massif is composed of a pre-Variscan polyorogenic and polymetamorphic basement (mainly gneisses, schists, migmatites and amphibolites) intruded during two phases by Variscan granitoids (Labhart 1999). The Gotthard massif is bordered in the north by a stratigraphic contact with Permo-carboniferous and Mesozoic sediments of the Urseren-Gravera-zone (Wyss 1986). This northern contact is locally strongly tectonized. In the south, the Gotthard massif is in contact with steeply dipping para-autochtonous metasediments (schists, carbonate, gypsum/anhydrite) of the Piora and Nufenen zones (Herwegh and Pfiffner 1999).

During the Tertiary alpine collision, the Gotthard massif was affected by greenschist facies metamorphism with an increasing N–S grade. At its southern boundary, amphibolite facies conditions were reached (Frey et al. 1980; Labhart 1999). The formation of a penetrative Alpine foliation and of steeply dipping ductile shear zones that mainly strike NE–SW occurred in a compressive NW–SE directed stress field (Marquer 1990; Steck 1968b; Zangerl et al. 2006; Zangerl 2003). Towards the end of the Tertiary collision, the deformation mode gradually evolved from ductile to brittle. Analyses of the interrelationship between brittle fault zones and meso-scale fractures indicate that during an early stage of brittle faulting, the stress regime changed from compression to strike-slip (Zangerl 2003;

Zangerl et al. 2006). The stress conditions prevailing during the formation of these brittle faults are not well constrained, but suggest a horizontal maximum principle effective stress direction striking about NE–SW and a minimum compressive principal stress direction in NW–SE direction. According to Lützenkirchen (2002), brittle faulting in the Gotthard massif occurred preferentially along pre-existing ductile shear zones under temperatures in the range of 250–200°C. Compared to the Central Aar massif, the Central Gotthard massif clearly shows more abundant and intensive brittle deformations along pre-existing joints and ductile faults (Zangerl et al. 2006).

Lützenkirchen (2002) demonstrated that in the Bedretto leg of the Furka base tunnel (Switzerland,) most of the deep inflows are related to the damage zones around fault zones, and that the flow contributed by individual joints not related to fault zones is negligible. He also observed that brittle faulting in the Gotthard massif often overprinted ductile shear zones and that the fault zones with higher flow rates always showed slickenside striations on shear fractures. Lützenkirchen (2002) divided fault zones and shear zones into six different types:

1. Ductile shear zones showing mylonitic and/or densely spaced foliation planes
2. Ductile shear zones overprinting lamprophyre and aplitic dikes
3. Brittle-ductile shear zones intensely fractured within ductile shear zones

Table 2 Basic tunnel and gallery information: Furka base tunnel, Gottard SBB, Gotthard A2 highway tunnel

| Tunnel name | Furka base tunnel | | Gotthard SBB | Gotthard A2 highway tunnel | |
Tube/gallery name	Realp leg	Bedretto leg	Railway tunnel	Security gallery	Main gallery
References	[a]	[a]	[b, c]	[b, d]	[b, d]
Excavation date	1973–1978	1973–1978	1872–1880	1980	1980
Survey date	From 1975	–	–	–	–
Delay	3 weeks–months	3 weeks	Months–years	1 day–4 months	3 weeks
Portal location(s) and elevation(s) [m]	Realp 1,550	Bedretto 1,480	Goeschenen 1,106 Airolo 1,142	Goeschenen 1,080 Airolo 1,146	Goeschenen 1,080 Airolo 1,146
Inflow reported by	Classes	Classes	Classes/rates	Classes	Classes
Drip. zone classes	LDZ/HDZ	LDZ/HDZ	LDZ/HDZ	LDZ/HDZ	LDZ/HDZ
Assigned rates [l/s]	0.001/0.01	0.001/0.01	0.02–0.05/0.19–0.49	0.01/0.1	0.01/0.1
Inflow classes [l/s]	<1/1–10/>10	<1/1–10/>10	N section/S section	<0.1 (N section only)/ 0.1–1/ >1	<0.1 (N section only)/ 0.1–1/ >1
Assigned rates [l/s]	0.3/3/25	0.3/3/25	–	0.03/0.3/3	0.03/0.3/3
Reported rates [l/s]	–	–	1.9–2.2/3.2–4.9	–	–
Rate error [l/s]	$\Delta Q = 2Q$	$\Delta Q = 2Q$	$\Delta Q = 3Q$	$\Delta Q = 2Q$	$\Delta Q = 2Q$

LDZ light dripping zone, *HDZ* heavy dripping zone

[a] Keller and Schneider (1982); Schneider 1985, unpublished report, see Table 1

[b] Schneider 1979, unpublished report, see Table 1

[c] Stapff 1882, unpublished report (see Table 1); Winterhalter and Dal Vesco 1961, unpublished report (see Table 1)

[d] Wanner 1982, unpublished report (see Table 1)

4. Brittle-ductile shear zones, wide, intensely fractured outside ductile shear zones
5. Brittle fracture zones
6. Brittle fault zones, narrow, intensely fractured and deformed

This showed that 90% of the estimated total flow rate to the deeper tunnel section was related to types 4 and 5. This observation is also compatible with the majority of inflows in the entire Gotthard massif study area.

Data set description

Data sources

The main part of the data used for the present study comes from the geological survey of 23 tunnels and galleries located in the Aar and the Gotthard massifs. References for the data sources of the individual tunnels are given in Tables 2–7. In addition to these project reports, this study also includes important data and findings from four PhD dissertations completed at the Swiss Federal Institute of Technology (ETH Zurich) in the same study area (Laws 2001; Lützenkirchen 2002; Ofterdinger 2001; Zangerl 2003). These research investigations give more detailed insight into the type and properties of water-conducting structures in the Aar and Gotthard massifs.

Data base parameters, and data processing and reliability

Tables 2−7 and Fig. 3 give the basic information for each tunnel or gallery which has been considered in the present study. The oldest document used is a report from Stapff 1882, unpublished report (see Table 1) on the construction of the Gotthard SBB (Schweizerische Bundesbahnen,

Swiss Federal Railways) railway tunnel and the most recent is a report from Schneider 1985, unpublished report (see Table 1) on the Furka base tunnel. Data from more recent tunnel constructions in the area, e.g. the Gotthard base tunnel, or the Grimsel hydropower system expansions (Aar massif), will be discussed in detail in subsequent papers. The quality and type of documentation from more than 100 years of underground construction is highly heterogeneous. For this reason, and in order to compare continuous parameters (e.g. depth) with discontinuous parameters (e.g. inflow rate), data had to be homogenized before being analyzed. This was mainly done by integrating each parameter over 100-m-long tunnel sections. The integration process has mainly two consequences. It first smoothes the parameters' variability

Table 3 Basic tunnel and gallery information: KW Amsteg, KW Lucendro

| Tunnel name | KW Amsteg | KW Lucendro |
Tube/gallery name	Supply gallery	Pressure gallery
References[a]	SBB Druckstollenkomission 1923	Winterhalter 1949b
Excavation date	–	–
Survey date	–	–
Delay	3 weeks	–
Portal location(s) and elevation(s) [m]	Pfaffensprung 791 Amsteg 530	Lucendro 2,033 Airolo 1,768
Inflow reported by	Classes	Classes
Drip. zone classes	DZ	DZ
Assigned rates [l/s]	–	0.01
Inflow classes [l/s]	Continuous inflow	Not reported
Assigned rates [l/s]	2.2	–
Reported rates [l/s]	–	–
Rate error [l/s]	–	–

DZ dripping zone

[a] Unpublished reports (see Table 1)

Table 4 Basic tunnel and gallery information: KW Goeschenen and KW Wassen

Tunnel name	KW Goeschenen			KW Wassen
Tube/gallery name	Pressure drift	Furkareuss supply gallery	Voralpreuss supply gallery	Supply gallery
References[a]	Winterhalter 1969b	Winterhalter 1969b	Winterhalter 1969a	Winterhalter 1969a
Excavation date	–	1956–1958	1956–1957	–
Survey date	1958	1958	1958	–
Delay	–	3 weeks	3 weeks	–
Portal location(s) and elevation(s) [m]	Goescheneralp 1,690 Goeschenen 1,100	Furkareuss 1,800 Goescheneralp 1,792	Voralpreuss Goescheneralp 1,792	Close to Wassen ~796
Inflow reported by	Classes	Classes	Classes	Classes
Drip. zone classes	LDZ/HDZ	DZ	LDZ/HDZ	Not reported
Assigned rates [l/s]	0.001/0.01	0.01	0.001/0.01	–
Inflow classes [l/s]	Continuous inflow	<0.1/0.1–1/>1	–	Continuous inflow
Assigned rates [l/s]	2.2	0.03/0.3/3	–	2.2
Reported rates [l/s]	–	–	Yes	–
Rate error [l/s]	–	$\Delta Q = 2Q$	$\Delta Q = Q/2$	–

[a] Unpublished reports (see Table 1)

along the different tunnels, and second, decreases the variance of the different parameter distribution.

Figure 3 shows the main hydrogeological parameters of each tunnel and gallery which have been compiled in a data base in a standardized format. All plots show the geological units (abbreviations according to Table 8) and the location of their boundaries, the number of dripping zones (divided into light or heavy dripping zone class) per 100-m interval, continuous tunnel inflow rates per 100-m interval, the depth and the angle between the main rock fabric (i.e. alpine foliation) and the tunnel axis. The continuous rate term is used as opposed to the dripping rate term. It refers to inflows that present a continuous water jet, whereas dripping rates are related to smaller inflows that have been reported as dripping zones from the tunnels. The key properties for further inflow analysis (Tables 2–7 and Fig. 3) are explained in the following.

Date of the tunnel excavation and hydrogeological survey
The survey date reported in Tables 2–7 is the date of the inflow rate measurements. The delay is the estimated time difference between the excavation date and the inflow measurement date at a given location along the tunnel. This delay is important information for the quantitative inflow rate analysis, but the delays are often not known or only roughly estimated (Tables 2–7). In most cases the

delay is several weeks to months, i.e. most of the rates reported in the data base and in Fig. 3 are close to steady state rates. Exceptions to this rule are discussed later (see section Exceptionally high tunnel inflow rates) and include, for example, the high inflows (110 and 150 l/s) to the Security gallery of the Gotthard A2 tunnel at Tm 9935 and 9910, where inflow rates, as measured by Lützenkirchen (2002), are on the order of 8 l/s. Tm stands for tunnel meters from a given reference point. In the case of the Gotthard A2 tunnel, the reference point is the northern portal (Fig. 3d).

Tunnel geology, location, orientation, elevation and depth
The location of each tunnel and gallery within the Aar and Gotthard massifs, and their elevation, orientation and depth are included in Figs. 2 and 3 and in Tables 2–7. The tunnels and galleries are well distributed over the study domain. The majority of the tunnels and galleries have a N–S orientation, i.e. an orientation perpendicular to the main Alpine structures. The portal elevation of each tunnel and gallery ranges between 530 m (KW Amsteg supply gallery) and 2,033 m (KW Lucendro pressure gallery). KW stands for "Kraftwerk" and means power plant in German. The different geological units crossed by each tunnel and gallery are reported in Figs. 2 and 3 with

Table 5 Basic tunnel and gallery information: Gas Transit

Tunnel name	Gas Transit		
Tube/gallery name	Urweid gallery	Gstelli gallery	Obergesteln gallery
References	Schneider (1974)	Schneider (1974)	Schneider (1974)
Excavation date	1972	1972–1973	Feb 1972—May 1973
Survey date	March 1973	1973	–
Delay	3 weeks	3 weeks	Several months
Portal location(s) and elevation(s) [m]	Close to Urweid ~800	Close to Guttannen ~1,150	Close to Obergesteln ~1,350
Inflow reported by	Classes	Classes/rates	Classes
Drip. zone classes	DZ	DZ	DZ
Assigned rates [l/s]	0.01	0.01	0.01
Inflow classes [l/s]	<1/>1	–	–
Assigned rates [l/s]	0.3/3	–	–
Reported rates [l/s]	–	Yes	Yes
Rate error [l/s]	$\Delta Q = 2Q$	$\Delta Q = 2Q$	$\Delta Q = Q$

Table 6 Basic tunnel and gallery information: KW Oberhasli and KW Ritom

Tunnel name	KW Oberhasli		KW Ritom	
Tube/gallery name	Gadmenwasser supply gallery	Handegg supply gallery	Unteralpreuss supply gallery	Garegna supply gallery
References[a]	–	Grundner 1942	Hügi 1961	Winterhalter 1957
Excavation date	–	–	1955–1958	1947–1955
Survey date	–	–	–	–
Delay	3 weeks	3 weeks	3–39 months	
Portal location(s) and elevation(s) [m]	Gadmental 1,342 Handegg gallery 1,290	Handegg ~1,400 Innertkirchen ~625	Unteralpreuss Lake Ritom ~1,850	
Inflow reported by	Classes	Classes/rates	Classes/rates	Classes
Drip. zone classes	–	–	LDZ/HDZ	–
Assigned rates [l/s]	–	–	0.001/0.1	–
Inflow classes [l/s]	Continuous inflow	Continuous inflow	–	Continuous inflow
Assigned rates [l/s]	5	0.6	–	5
Reported rates [l/s]	–	NW part only	Yes	–
Rate error [l/s]	–	$\Delta Q = Q/2$ or $2Q$	$\Delta Q = Q/2$	$\Delta Q = 2Q$

[a] Unpublished reports (see Table 1)

abbreviations defined in Table 8 and Fig. 2. The geological units relate to different rock types and tectonic units. The geological map has been modified from Labhart (1999). For each tunnel and gallery, the depth has been computed by subtracting the elevation of the gallery from the elevation of the ground surface based on a digital elevation model. The maximum depth ranges between 224 m (Gas Transit pipeline—Urweid drift) and 1,680 m (Gotthard SBB railway tunnel). The depth of every tunnel and gallery is also seen in Fig. 3.

Tunnel inflows
The tunnels discussed have hardly ever been grouted (pressures and flow velocities are too high at the tunnel depths considered) and the tunnel inflow rates, therefore, represent induced flows of natural features. Geological and hydrogeological data are heterogeneous because they come from different projects and have been collected by different persons at different times. This is especially true for inflow data which have been reported in basically two different ways. The largest amount of tunnel and gallery

inflow has been reported by classes of inflow rate only. A smaller part has been reported by measured or estimated inflow rates. For quantitative analysis, continuous inflows reported by classes of rate have been assigned a mean rate. Tables 2–7 give information about how inflows have been reported for each tunnel and gallery. When reported by classes, the assigned mean rate value assumed for each class is also mentioned. For example, the Gotthard A2 highway tunnel continuous inflows have been reported by three classes: inflows smaller than 0.1 l/s, inflows between 0.1 and 1 l/s and inflows bigger than 1 l/s. Then, inflows from each class have been assigned a mean rate of 0.03, 0.3 and 3 l/s respectively. If possible, when only one class of inflow was reported, the assigned mean rate value has been computed by dividing the cumulate flow at the portal by the number of continuous inflows contributing to the flow. Finally, when no cumulate flow was available, inflows have been assigned mean rate values based on the geometric mean of the class boundaries, assuming that rate values within a given class are lognormally distributed or, more generally, that inflow rates are lognormally distributed.

Table 7 Basic tunnel and gallery information: KW Vorderrhein

Tunnel name	KW Vorderrhein				
Tube/gallery name	Val Val – Curnera gallery	Nalps – Sedrun gallery	Curnera – Nalps gallery	Sedrun – Medels gallery	Santa Maria – Nalps gallery
References	[a]	[a]	[a]	[a]	[a]
Excavation date	-	-	-	-	-
Survey date	-	-	-	-	-
Delay	3 weeks	3 weeks	3 weeks	3 weeks	3 weeks
Portal location(s) and elevation(s) [m]	Val ValCurnera ~1,950	Nalps ~1,900; Sedrun ~1,400	Curnera ~1,950; Nalps ~1,900	Sedrun ~1,400Medels	Santa MariaNalps ~1,900
Length [m]	5,700	3,600	3,600	6,200	8,600
Inflow reported by	rates	rates	rates	rates	rates
Drip. zone classes	-	=	=	=	=
Assigned rates [l/s]	-	=	=	=	=
Inflow classes [l/s]	-	=	=	=	=
Assigned rates [l/s]	-	-	-	-	-
Reported rates [l/s]	Yes	Yes	Yes	Yes	Yes
Rate error [l/s]	$\Delta Q = 2Q$	ΔQ	ΔQ	ΔQ	ΔQ

[a] Schneider 1972, unpublished report, see Table 1, Schneider (1981)
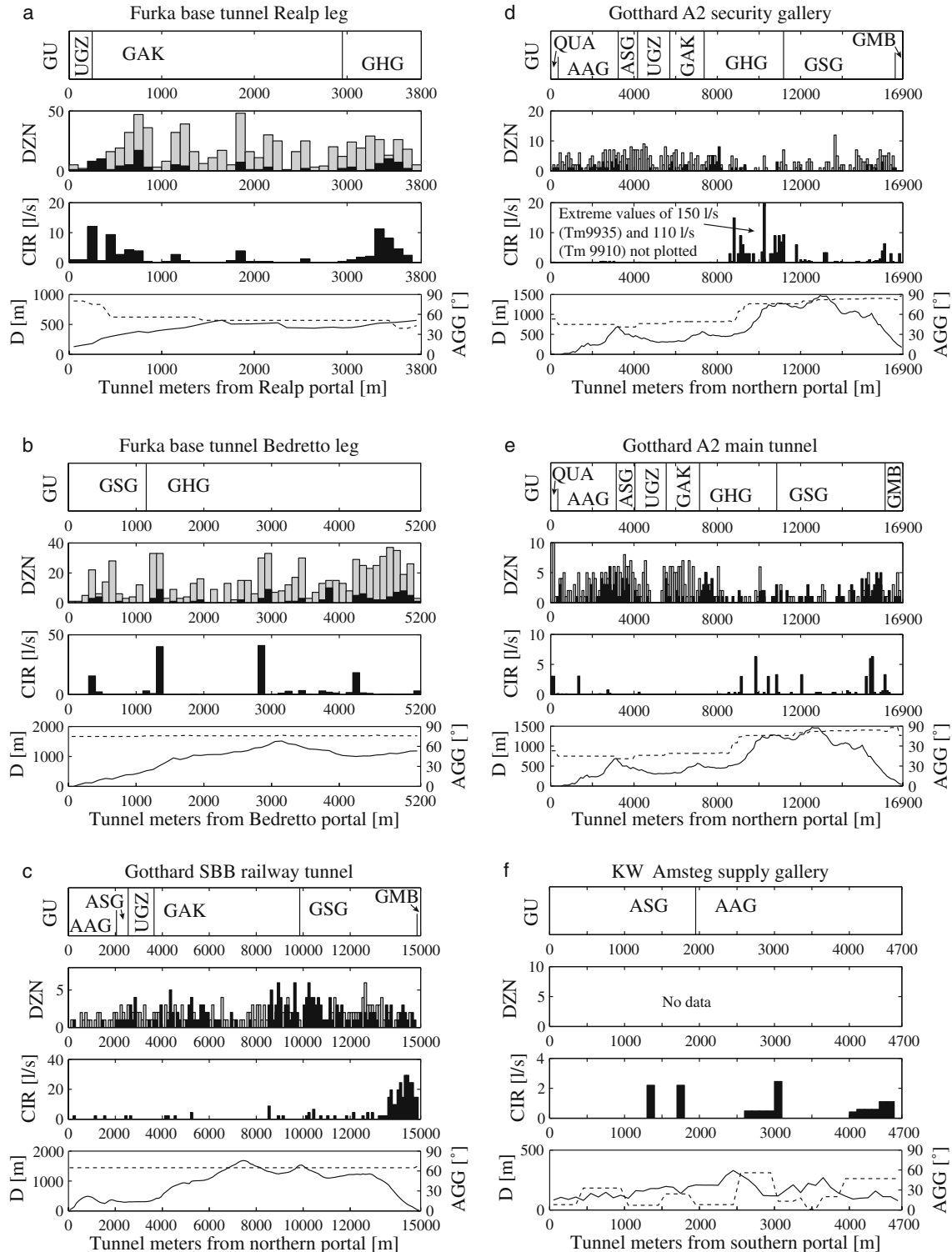
Fig. 3 Location plot of the geologic boundaries (*GU*) along the tunnel, bar chart of the number of dripping zones (*grey*: light dripping zone; *black*: heavy dripping zone) per 100 m of tunnel (*DZN*), bar chart of the continuous inflow rate per 100 m of tunnel (*CIR*) and plot of the depth (*D*, continuous line) and the angle between the tunnel axis and the Alpine main foliation (*AGG*, *dashed line*) along the tunnel for all underground excavations discussed in this paper. **a**–**v** The labels of each part correspond to the labels for the tunnels listed in the Fig. 2 caption

When localized inflows become too small for hand measurements of inflow rates with a bucket and watch, i.e. when individual continuous water-jets break down, dripping zones are recorded by the on-site geologists. These dripping zones are sometimes mapped in two classes (heavy and light). Dripping inflows have also been assigned rates according to their class (0.01 and 0.001 l/s).

A rate error has been assumed for each rate value that was used for later transmissivity estimation (Tables 2–7). The assumed error is proportional to the rate and quality
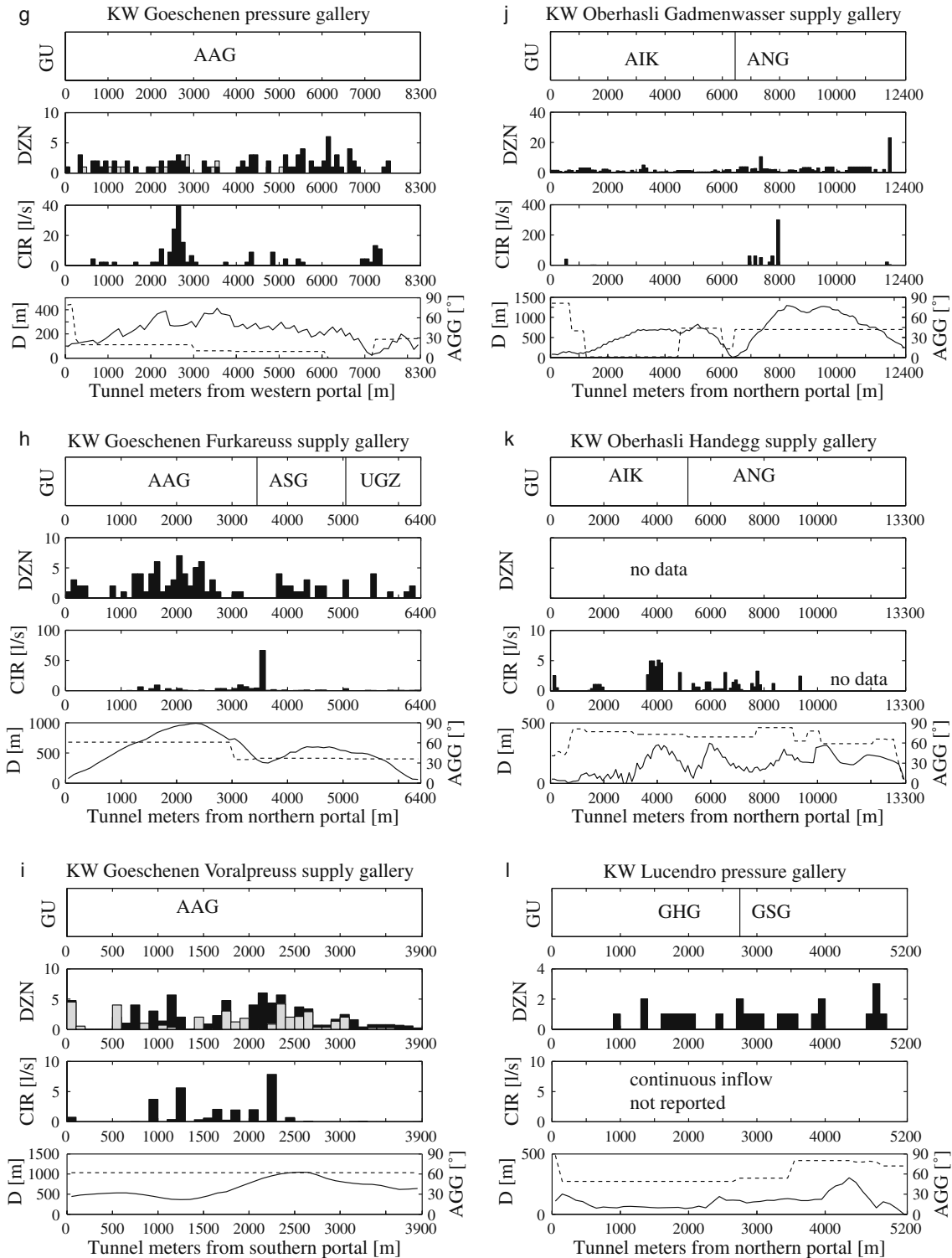
Fig. 3 (continued)

of the value that has been reported. The quality of the value is based on the measurement method used and the type of data reported. When the rate has been quantitatively reported, the rate error is assumed to be equal to half of the rate value. When inflows have been reported by classes, the rate error is estimated to be equal to two or three times the rate value.

Exceptionally high tunnel inflow rates

In the tunnels and galleries discussed here, a few exceptionally high singular tunnel inflow rates have been observed. These high inflows have important scientific and practical implications (they control the total inflow rate, the design of drainage measures, and safety considerations); so therefore their geologic and topographic
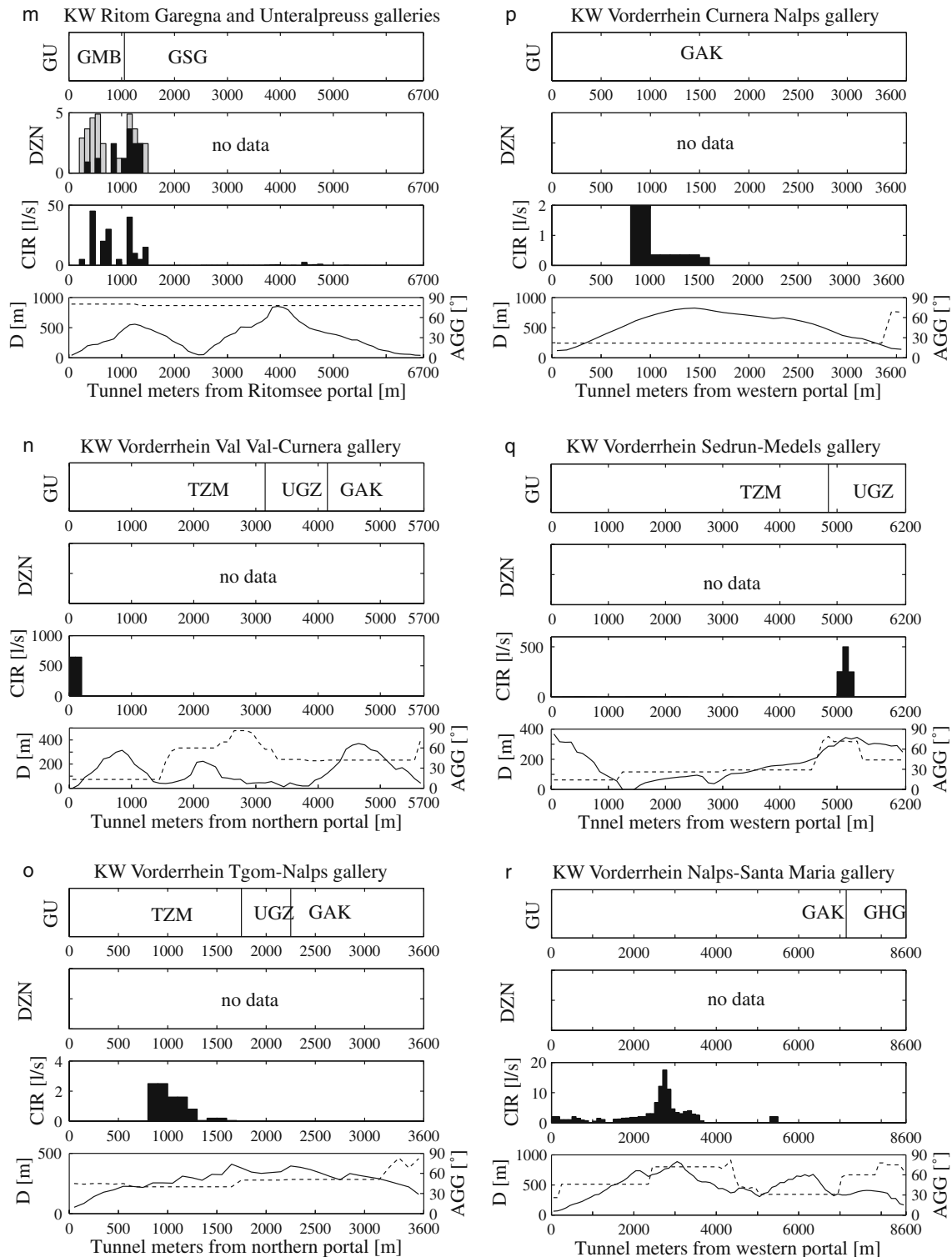
Fig. 3 (continued)

conditions are presented here in detail. Most of these high values are not shown in Fig. 3 because they represent initial (early time) inflows which strongly decreased with time. Using them for quantitative analysis would require exact knowledge of the inflow time.

In the *Bedretto leg* of the Furka base tunnel, up to 57 l/s of water were initially flowing into the tunnel during

excavation from Tm 2815 to Tm 2850 in the Rotondo granite (GHG). Based on the descriptions of this tunnel in Keller and Schneider (1982) and Lützenkirchen (2002), this large inflow is related to a brittle fault zone. In the Bedretto gallery, exceptionally high initial inflow rates were also recorded close to the southern portal (up to 130 l/s initially between Tm 180 and Tm 360), where

Table 8 Geological units and their corresponding abbreviations

Tectonic unit	Geological unit	Abbreviation
Aar massif	"Innertkirchner-Kristallin"	AIK
	Northern "Altkristallin"	ANG
	Granite sensu lato	AAG
	Southern "Altkristallin"	ASG
Tavetsch massif		TZM
Gotthard massif	"Urseren-Gravera-Zone"	UGZ
	Northern "Altkristallin"	GAK
	Variscan intrusives	GHG
	Southern "Altkristallin"	GSG
	Southern sedimentary cover	GMB

toppling of steeply dipping foliation planes resulted in a strongly increased rock mass hydraulic conductivity (Keller and Schneider 1982). In July 1875, in the *Gotthard SBB railway tunnel*, after excavation of the first 2,100 m from the southern portal in the Tremola series (GSG), a cumulate inflow rate of 130–350 l/s, taking place in the strongly fractured meta-sediments of the Tremola series, was measured at the portal over a long period of time (October 1873–July 1879). The depth is limited (0–750 m) and toppling occurs again at ground surface and also at tunnel elevation close to the portal. In the *Gotthard A2 security gallery*, two initial inflows of 150 l/s (Tm 9935) and 110 l/s (Tm 9910) were encountered at greater depth, occurring in cross-cutting fault zones of the Gamsboden granite (GHG) and were intensively studied by Zangerl et al. (2006) and Lützenkirchen (2002). Today the inflow rate from this tunnel section is about 8 l/s. In the *Goeschenen Voralpreuss supply gallery*, at Tm 1340 in the Aar granite, an inflow with an initial maximum rate of 140 l/s was reported in a place where the depth is below 500 m. The high (initial?) inflow value of the *Furkareuss supply gallery* (60 l/s) must be related to the relative close proximity to ground surface, large scale tectonic faulting (Eckart et al. 1983; Steck 1968b), and unloading features observed along the Urseren valley. In the *KW Oberhasli Gadmenwasser supply gallery*, an early time inflow of 300 l/s was observed in a brittle fault zone of 1-m width in gneisses of the Aar massif (ANG). The inflow location has a depth of about 800 m. In *KW Ritom Unteralpreuss supply gallery*, 140 l/s was initially flushed out of a clayey joint when it was intersected by the excavation at Tm 2306. This inflow is found in heterogeneous gneisses of the southern Gotthard massif at a shallow depth. The sugar-grained dolomites found in the southern sediment cover of the *Garegna supply gallery* show high inflows ranging between 120 and 150 l/s over a total section length of about 1,000 m. Close to the northern portal of the *KW Vorderrhein Val Val—Curnera reservoir supply gallery*, a maximum (initial?) inflow rate of 1,300 l/s occurred within a 200-m wide cataclastic fault zone in the gneisses of the Tavetsch massif close to the northern border to the Aar massif (possibly the same regional tectonic structure responsible for the large inflows to the Furkareuss supply gallery). In the *KW Vorderrhein Sedrun—Medels gallery*, 1,000 l/s rushed in from a 200-m-long tectonized section in the transition area from Triassic sediments to

Permo-Carboniferous gneisses of the Urseren-Gravera zone (Tm 5.050–5.250). Due to the shallow depth, the evaporitic sediments (anhydrite/gypsum) occurring within this succession are presumably affected by karstic dissolution phenomena. Finally, in the Gas Transit pipeline *Obergesteln gallery*, strong initial inflows were recorded in the northern 1,000 m, with the highest individual inflow of 110 l/s (Tm 550) encountered at 300 m depth (Klemenz 1974). Again, this entire section shows relatively deep (>300 m) toppling of Variscan gneisses (GHG), and the initial inflow rates quickly decreased to much lower values (10–50 l/s over the entire section after 1 year).

Statistical distribution of tunnel inflow rates

Inflow rate distribution as a function of geological unit

In the statistical analysis of the distribution of inflow rate, only tunnel inflow rate data with a sufficient quality have been taken into account. Data from the following tunnels or galleries have been excluded: KW Amsteg supply gallery, Goeschenen pressure gallery, KW Lucendro pressure gallery, KW Ritom Garegna supply gallery, KW Vorderrhein Sedrun-Medels gallery, KW Wassen supply gallery and Gas Transit Gstelli gallery.

As discussed earlier, rate data have been divided into three different sets, based on continuous inflows, dripping zones, and "dry" tunnel sections. The rates of continuous inflows, summed over 100-m-long tunnel intervals, include all mapped continuous inflows shown in Fig. 3, but exclude extreme values and continuous inflows smaller than 0.01 l/s. Inflows with a rate lower or equal to 0.01 l/s have not been systematically reported and for that reason have been excluded.

The second set is derived by assigning a value to each dripping zone according to its strength and by summing these values again over 100 m-long tunnel intervals. The values assigned are 0.001 and 0.01 l/s for low and heavy dripping zones respectively. Assigning rate values to dripping zones is problematic for the given data set. An attempt to relate the dripping zones to inflow rates in Bedretto gallery can be found in Lützenkirchen (2002), but as the definition of dripping zones varies between individual tunnel geologists, the generalization of his assessment remains questionable. Lützenkirchen estimated flow rates for dripping zones lower than the values assigned in this study. Modifying the assigned rate values results in a shifting and/or rescaling of the dripping-rate distribution. However, it does not significantly modify the total cumulative inflow rate from dripping and continuous inflows.

The last set of inflow rates used in this study is the mean inflow rate from "dry" tunnel sections (i.e. without dripping inflows), which is non-visible water inflow transported as water vapor through the tunnel ventilation. For the assessment of these rates, new air water vapor measurements from a 1,000-m-deep section of the Gotthard base tunnel near Sedrun (Fig. 2) could be used.

In this section, located north and south of the Sedrun shaft, individual vapor flow measurements from the west tube (W) and the east tube (E) were used. Both tube sections in the north (tubes NW, NE) are around 1,300 m long and located in the Tavetsch massif. The other two sections located south of Sedrun's shaft (tubes SW, SE) are around 2,300 and 2,500 m long respectively and belong to different geological units (see Fig. 2). While long sections of the north tubes are indeed "dry", the tubes in the south direction contain several dripping sections and a few continuous inflows. Details of the procedure used to compute the water vapor output are described later (see Appendix 2). The water vapor flow rate of each of the four tubes (NW, NE, SW, SE) has been divided by its length to obtain the flow rate per tunnel meter or hectometer. As shown in Table 9, the hectometric inflow rates are comparable to the smallest inflow rates reported for a single continuous inflow (0.01 l/s). The equivalent transmissivity and hydraulic conductivity values have also been computed by assuming a tunnel radius of 5 m and a differential head of 1,000 m. The different water vapor output parameters and resulting rate values are summarized in Table 9. These water-vapor rate values are mean values because the water-vapor flow has been integrated over more than 1,000 m of tunnel. Most probably this flow is not constant along the tunnel and a function of the local rock-mass hydraulic conductivity. Since the walls of NW and NE tubes are rather dry, the transmissivity (T) and hydraulic conductivity (K) values derived from these sections can be considered as mean T- and K-values for the matrix, here defined as the rock embedding these tunnel "dry" sections without dripping zones and continuous inflows.

The histogram of Fig. 4 shows the distribution of the continuous inflow rates (black bars) and the dripping inflow rates (grey bars) for all the geological units combined. The binning is logarithmic and the bin size is chosen to be equal to the size of the rate classes (one log
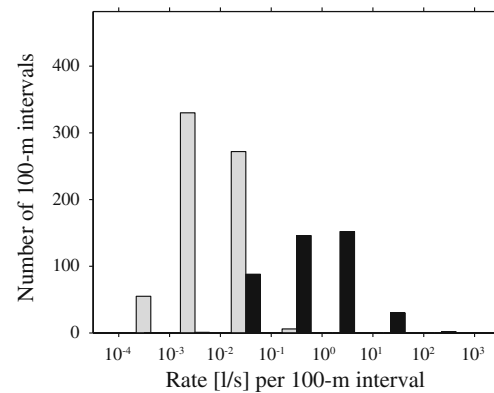

Fig. 4 Histogram showing dripping inflow rates (*grey*) and continuous inflow rates (*black*) for all geologic units

cycle in this case) in order to avoid a discontinuous or incomplete representation of the rate distribution. Both rate distributions look lognormal and overlap each other. Due to sampling limits, the surveyed rate distribution is truncated toward the low rate values. Although the dripping-inflow-rate distribution is more uncertain than the continuous-inflow-rate distribution, combining them has the advantage to extend the sampled rate distribution towards the low rate values. The surveyed rate distribution per 100 m tunnel section for all geological units extends over seven orders of magnitudes from 10^{-4} to 10^{4} l/s. Figure 5 shows the undifferentiated-inflow-rate distribution when dripping and continuous flow rates are summed over each individual 100-m interval. The resulting distribution is again close to a lognormal distribution.

Similar histograms have been created for each geological unit and are shown in Fig. 6. The histograms rarely follow a lognormal distribution and are sometimes scattered and asymmetric: the right (higher rate) tail of the distribution is often longer than the left tail. There is no evident correlation between distributions of similar lithologies. For example, the highest maximum rate is

Table 9 Air water vapor content parameters and results

| Parameters	Units	Tunnel sections			
		SW	SE	NW	NE
Air volumetric flow rate	A [m³/s]	42	43.8	45	44.9
Absolute pressure	P [Pa]	96,200	96,200	96,300	96,300
Absolute temperature	Temp [K]	300.9	299.6	297.2	298.4
Water vapor partial pressure	P_w [Pa]	2,060	1,300	1,730	1,600
Air water content No. 1	c_1 [kg/kg]	0.0127	0.0100	0.0084	0.0107
Air water content No. 2	c_2 [kg/kg]	0.0189	0.0152	0.0125	0.0147
Tunnel section length	L [m]	2,300	2,500	1,300	1,300
Gas constant for air	R_L [J/(kg × K)]	287.1	287.1	287.1	287.1
Tunnel radius	r [m]	5	5	5	5
Hydraulic head	h [m]	1,000	1,000	1,000	1,000
Gas constant for wet air	R_f [J/kg × K]	289.4	288.6	289.1	288.9
Density	ρ [kg/m³]	1.10	1.11	1.12	1.12
Vapor mass flow rate	m [kg/s]	46.4	48.7	50.4	50.2
Air water content difference	Δc [kg/kg]	0.0062	0.0052	0.0041	0.0040
Vapor volumetric flow rate	V [l/s]	0.29	0.25	0.21	0.20
Vapor vol. flow rate per m	V_2 [l/s/m]	1.25×10^{-4}	1.01×10^{-4}	1.59×10^{-4}	1.54×10^{-4}
Vapor vol. flow rate per 100 m	V_3 [l/s/hm]	0.01	0.01	0.02	0.02
Transmissivity per 100 m	T [m²/s]	1.19×10^{-8}	9.66×10^{-9}	1.52×10^{-8}	1.47×10^{-8}
Hydraulic conductivity	K [m/s]	1.19×10^{-10}	9.66×10^{-10}	1.52×10^{-10}	1.47×10^{-10}
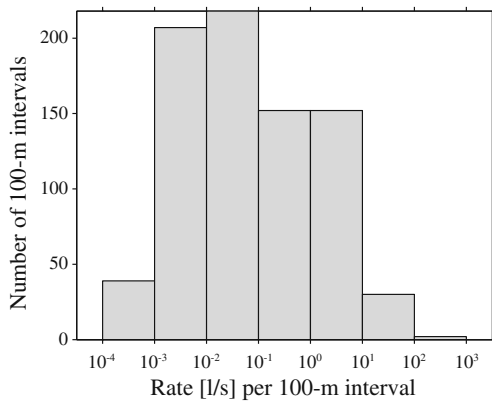
Fig. 5 Histogram showing dripping and continuous inflow rates for all geologic units

found for the Gotthard massif granites (GHG), whereas the lowest maximum rate is observed for the Aar massif granites (AAG).

Inflow rate distribution as a function of depth

For the analysis of the dependence of inflow rate as a function of depth, the same tunnels in the previous section (see section Inflow rate distribution as a function of geological unit) have been excluded from the data set. Only the first set of data (continuous inflows) have been

used, and 100-m intervals with inflow rates lower or equal to 0.01 l/s have been assigned the rate value 0.01 l/s to account for the dripping and the moisture evaporation. This simplification can lead to overestimation of inflow rates and a bias in the rate distribution.

For all geological units combined, and for each geological unit, five different plots (Figs. 7 and 8) have been generated to study the inter-dependency between inflows and depth. As data are discrete and non-homogeneously distributed with depth, a sampling window (moving average) of 200 m depth has been used in all the plots for five different rate classes (0.01, 0.01–0.1, 0.1–1, 1–10 and >10 l/s). The first type of plot shows the total number of 100-m intervals (NI) of the different rate classes versus depth in order to visualize the variability of sampling frequency with depth. The more data are available, the more the results in the next four plots are significant. The second plot type shows the total number of 100-m intervals of the different rate classes divided by the total number of all 100-m intervals as a function of depth; the result is the proportion of the different classes (PC) among the sampled intervals. The third plot type shows the total inflow rate (TIR) of the different rate classes versus depth. For the fourth plot type, the total inflow rate of the different classes is divided by the total inflow rate and plotted versus depth; this gives the contribution to the total flow (CC) of each class versus
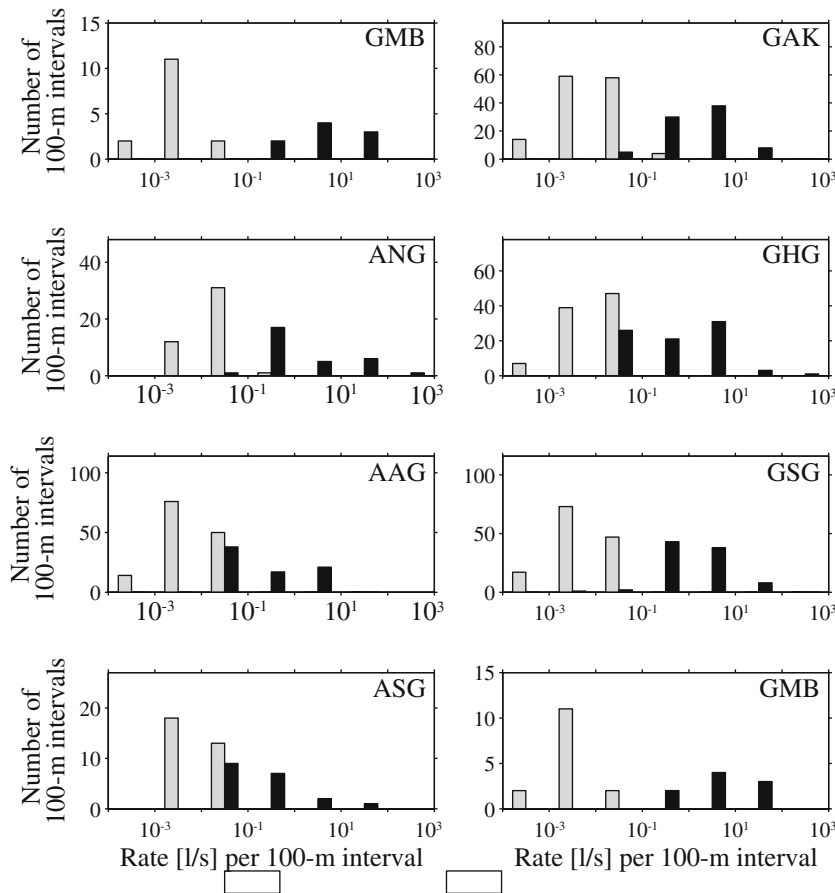

Fig. 6 Histogram showing dripping inflow rates (*grey*) and continuous inflow rates (*black*) for each geologic unit
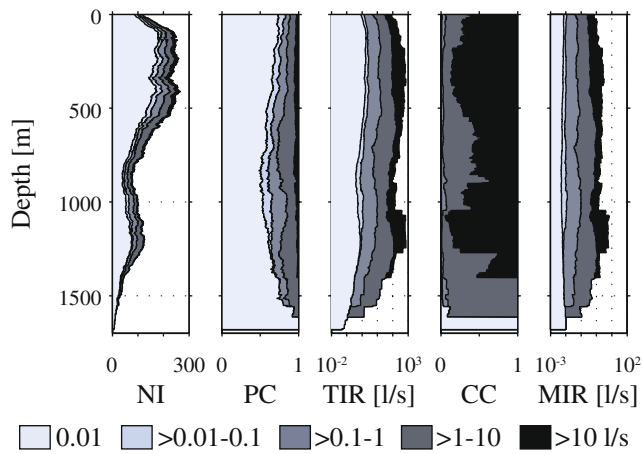
Fig. 7 All geologic units: Moving average (200 m) of the number of intervals (*NI*) of the different rate classes (0.01, 0.01–0.1, 0.1–1, >10 l/s) with depth, moving average of the proportion of the different rate classes (*PC*) with depth, moving average of the total inflow rate (*TIR*) with depth, moving average of the class contribution (*CC*) to the total rate with depth and moving average of the mean inflow rate per 100-m interval (*MIR*) with depth

depth. Finally, the last plot type represents the total inflow rate of the different rate classes divided by the number of 100-m intervals of each class versus depth; the result is the total mean inflow rate (MIR) per 100-m interval of the different classes versus depth.

From the analysis of the plots for all geological units combined (Fig. 7), one can conclude that:

– PC: The relative proportion of the different inflow classes is nearly constant with depth
– NI: Apart from the artificial 0.01 l/s class, which includes 50–70% of the intervals, the most frequent is the 1–10 l/s class and the highest rate class (>10 l/s) is the less represented
– CC: More than 90% of the total flow rate is fed by intervals whose rate is bigger or equal to 1 l/s
– MIR: The mean inflow rate per 100 m interval amounts to about 2 l/s and is relatively uniform over long depth sections
– MIR: A section of extraordinary high mean-inflow rates appears between 1,050 and 1,250 m depth

Concerning the plots of the individual geological units (Fig. 8), one can conclude that:

– NI: The depth intervals with a significant amount of observations strongly varies with geological unit
– PC and MIR: The upper most 200–400 m of the AAG, ANG and GHG geological units show a low relative proportion of the highest rate classes and low mean inflow rates
– PC and MIR: In contrast, the upper most 200–400 m of the AIK, GAK and GSG geological units show a high relative proportion of the highest rate classes and high mean inflow rates
– PC and MIR: Below the uppermost interval, a general decrease of the highest rate classes proportion and of

the mean rates is observed in the ASG, GAK and GSG geological units
– MIR: The AAG unit shows a steady increase of the mean inflow rate down to 800 m depth
– MIR: No clear depth trend is observed in the mean rate of GHG and ANG units

Inflow spacing distribution along tunnels

The spacing distribution of continuous inflows has been analyzed along four tunnels and galleries where precise inflow localization was available (Masset and Loew 2007). This analysis shows that the spacing distribution of continuous inflows along the Realp leg of Furka base tunnel, the Gotthard SBB railway tunnel, the Gotthard A2 security gallery and the Goeschenen pressure drift are well fitted by power laws over ~1.5–2 orders of magnitude (Fig. 9). This illustrates the clustered distribution of continuous inflows along tunnels. In other terms, these appear in series separated by intervals where only dripping occurs and this pattern repeats at different scales.

Figures 10 and 11 show the spacing distribution of continuous inflows, heavy dripping inflows and light dripping inflows along Gotthard SBB railway tunnel and Goeschenen pressure drift. On both plots, it can be seen that, in contrast to continuous inflows, dripping zones are more evenly spaced and particularly light dripping inflows are well fitted by exponential functions. Thus, it appears that the spacing distribution of inflows along tunnels is a function of the inflow rate or type.

Major parameters controlling tunnel inflows

Tectonic overprint

In the central Aar and Gotthard massifs, the tectonic overprint has induced important multi-scale ductile and brittle deformations. Brittle tectonic overprint includes all types of fractures formed during and after the Alpine orogeny. In Figs. 7 and 8, the peaks in mean inflow rate always results from the presence of one or a few high-rate inflows at the intersection between the tunnel and zones of brittle deformation. For example, the deviation from the mean inflow rate shown in Fig. 7 in the depth interval of 1,050 to 1,250 m is related to the local occurrence of strong inflows from brittle faults in the ANG (KW Oberhasli Gadmenwasser supply gallery) and GHG geological units (Gotthard A2 security gallery). These deviations are superimposed on possible depth or lithology dependant trends in inflow rate. The strong brittle overprint of GHG (granites of the Gotthard massif) controls the inflow rate distribution and completely obscures the correlation between inflow rate and depth.

In contrast, the AAG geological unit (granites of the Aar massif) shows no significant peaks of the inflow rate and the lower brittle overprint of AAG compared to GHG allows the observation of a depth-dependant inflow rate. A general lower brittle tectonic overprint not only characterizes the AAG geological unit, but also the entire central Aar massif, with the exception of its southern margin
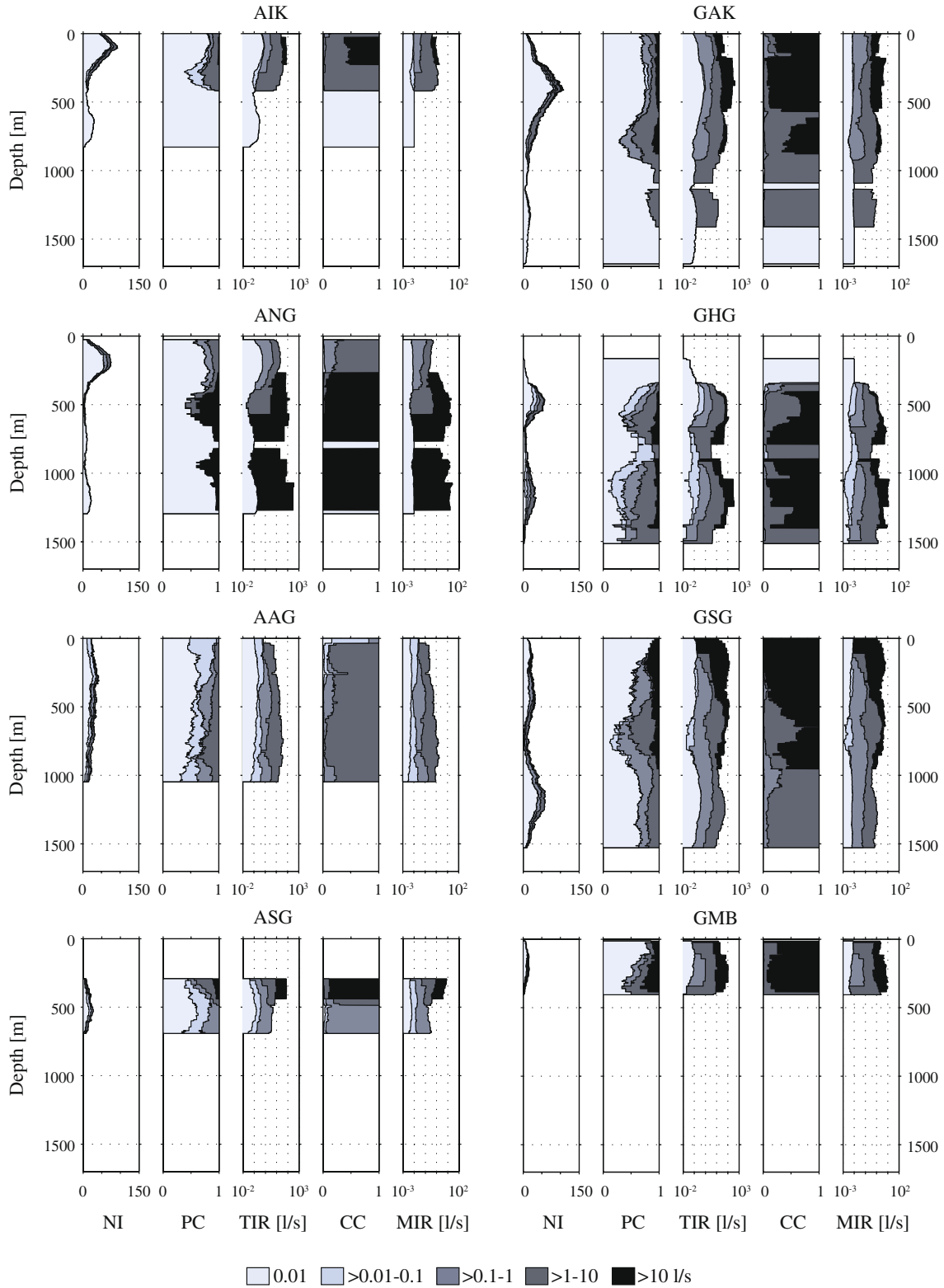
Fig. 8 Individual geologic units: Moving average (200 m) of the number of intervals (*NI*) of the different rate classes (0.01, 0.01–0.1, 0.1–1, >10 l/s) with depth, moving average of the proportion of the different rate classes (*PC*) with depth, moving average of the total inflow rate (*TIR*) with depth, moving average of the class contribution (*CC*) to the total rate with depth and moving average of the mean inflow rate per 100-m interval (*MIR*) with depth (see Table 8 for explanation of abbreviations)
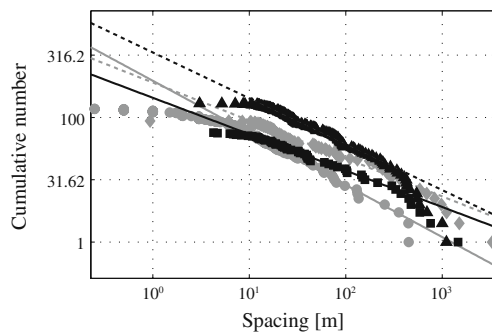
Fig. 9 Continuous inflow spacing distribution fitted by power laws along the Realp leg of Furka base tunnel (*grey circles, grey line*), the Gotthard SBB railway tunnel (*grey diamonds, dashed grey line*), the Gotthard A2 security gallery (*black triangles, dashed black line*) and the Goeschenen pressure drift (*black squares, black line*)

(ASG). Consequently, mean 100-m interval inflow rate values are lower for the Aar massif (2.6 l/s) than for the Gotthard massif (3.85 l/s).

Topography and unstable slopes

The systematic trend of increasing inflow frequencies and rates in the upper 100 to 400 m of Figs. 7 and 8 reflects partly unsaturated conditions in mountain slopes. In the study area, the upper 100–400 m below ground surface often show highly permeable rock masses composed of a dense partially interconnected pattern of open fractures (southern portal of SBB Gotthard, northern portal of gas transit Obergesteln, southern portal of Bedretto gallery). These open-fracture sets are composed of tectonic and near-surface unloading fractures (Bucher 2006; Zangerl et al. 2006). Fractures are opened by stress release and slope deformation phenomena, especially flexural and block toppling (Keller and Schneider 1982; Klemenz 1974). This induces a significant increase in fracture transmissivity. Depending on the local topographic and geologic situation, the upper most 100–400 m of rock can show saturated or unsaturated conditions before tunnel excavation, i.e. the absence of tunnel inflows in these sections do not imply low permeability rock masses. In fact, the initial tunnel inflow rates from such sections are often relatively high and decrease during the first days and
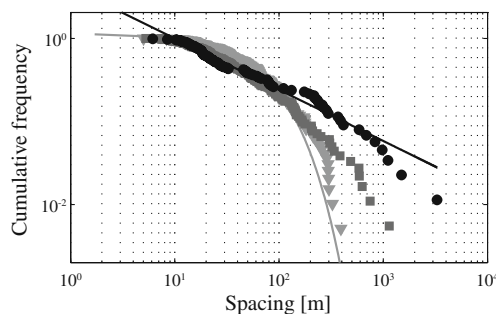

Fig. 10 Gotthard SBB railway tunnel spacing distributions of light dripping zones (*pale grey triangles*) fitted by an exponential curve (*pale grey curve*), heavy dripping zones (*dark grey squares*) and continuous inflows (*black circles*) fitted by a power law (*black line*)
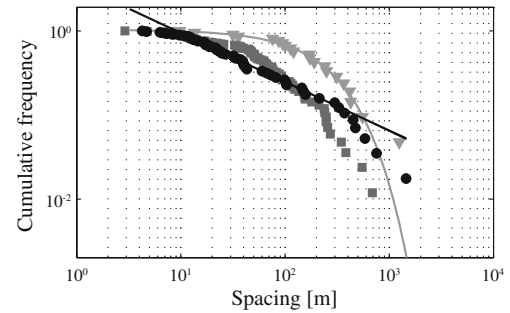

Fig. 11 Goeschenen pressure drift spacing distributions of light dripping zones (*pale grey triangles*) fitted by an exponential curve (*pale grey curve*), heavy dripping zones (*dark grey squares*) and continuous inflows (*black circles*) fitted by a power law (*black line*)

weeks dramatically due to lowering of the water table down to the elevation of the tunnel (Klemenz 1974; Loew et al. 2007). Late time inflows are small and strongly controlled by local and temporally varying groundwater recharge. As discussed earlier, most of the high initial inflows have not been included in the data base shown in Fig. 3.

Depth and lithology

The dependency between inflow rate and depth is most visible in the particular case of the AAG unit (granites of the Aar massif) because the tunnel sections crossing this unit did not encounter strong inflows that can be related to surface unloading or brittle faults (Fig. 8). This unit shows increasing inflow rates with depth (MIR in Fig. 8). However, this does not mean that granites are in general less affected by brittle tectonic or less permeable than gneisses since the GHG unit (granites of the Gotthard massif) shows strong inflow rate variations with depth due to brittle faulting.

Moreover, when comparing the Gotthard railway (SBB) tunnel (Fig. 3c) with Gotthard A2 security gallery (Fig. 3d), which run nearly parallel to each other at a lateral distance of up to 3 km, one can see that the high inflow rates found in the granitic section (GHG) of the A2 security tunnel have no equivalent in the gneissic section (GAK) of Gotthard railway tunnel. As inflows in both tunnels are controlled by brittle faults cross-cutting the tunnels at a high angle, it is suggested that brittle faulting in granites leads to more conductive structures than brittle faulting in gneisses.

Fracture transmissivities

Data processing and transmissivity models

To compute transmissivity values from tunnel inflows, only data with sufficient quality have been used. Data from the following tunnels and galleries are not included in the transmissivity analysis: KW Amsteg supply gallery, Goeschenen pressure gallery, KW Lucendro pressure gallery, KW Ritom Garegna supply gallery, KW Vorderrhein Sedrun-Medels gallery, KW Wassen supply gallery

and Gas Transit Gstelli gallery. Continuous inflow intervals with rates smaller or equal to 0.01 l/s have been excluded because small rates have not systematically been reported. As described earlier (see section Data set description), dripping zones have been assigned rates of 0.01 l/s or 0.001 l/s depending on their strength. Transmissivity values have been computed for each 100-m interval using three different analytical models depending on the hydrogeologic setting of the considered 100-m interval (Loew 2002). All models are 2D and assume that:

– The inflow is derived from an infinite planar layer oriented normal to the tunnel/gallery axes (vertical layer, fracture zone, fault or fault zone)
– The layer transmissivity is homogeneous and no leakage takes place between the layer and the surrounding rock
– The tunnel is radial and at a constant head controlled by atmospheric pressure
– The flow is governed by Darcy's law
– The inflow time of the rate reported in the data base corresponds to the delay time
– The rock mass specific storage is equal to 10^{-6} m^{-1} (only required for transient models)

The first model represents infinite acting radial flow (Fig. 12a) and can be approximated with the Jacob and Lohman (1952) solution for non-steady flow to a well of constant drawdown, assuming that the hydraulic head

drawdown is equal to the elevation difference between the tunnel and the water table (often approximated by ground surface). The radial flow model is the basic model applied to most of the productive 100-m tunnel intervals.

The second model is similar to the first one except that it is limited by a linear constant head upper boundary (Fig. 12b) under steady-state conditions. This model is applied instead of the first model when a recharging lake, a river or a Quaternary aquifer at the surface is suspected to maintain the water table at a constant level. For example, this model is used to compute transmissivity of a section of the Gotthard railway and A2 highway tunnels below the gravel aquifer of the Urseren valley. This model it is also used to compute the transmissivity from dripping rate values.

The third model derived from Doe (1991) is a solution for linear flow under a constant drawdown. It applies when the drying out of surface springs in direct response to the tunnel or gallery excavation demonstrates the drawdown of the water table down to the tunnel elevation and when linear horizontal flow normal to the tunnel axes is a reasonable approximation (Fig. 12c) (Klemenz 1974, Loew et al. 2007). The specific yield (S_y) is set to 0.01. This value has been derived by dividing the total amount of water drained into a section of the Obergesteln gallery by the volume of rock drained. The volume of water was measured and the volume of rock estimated from the position of dried out and unmodified surface springs (Loew and Masset 2008, unpublished report, see Table 1).
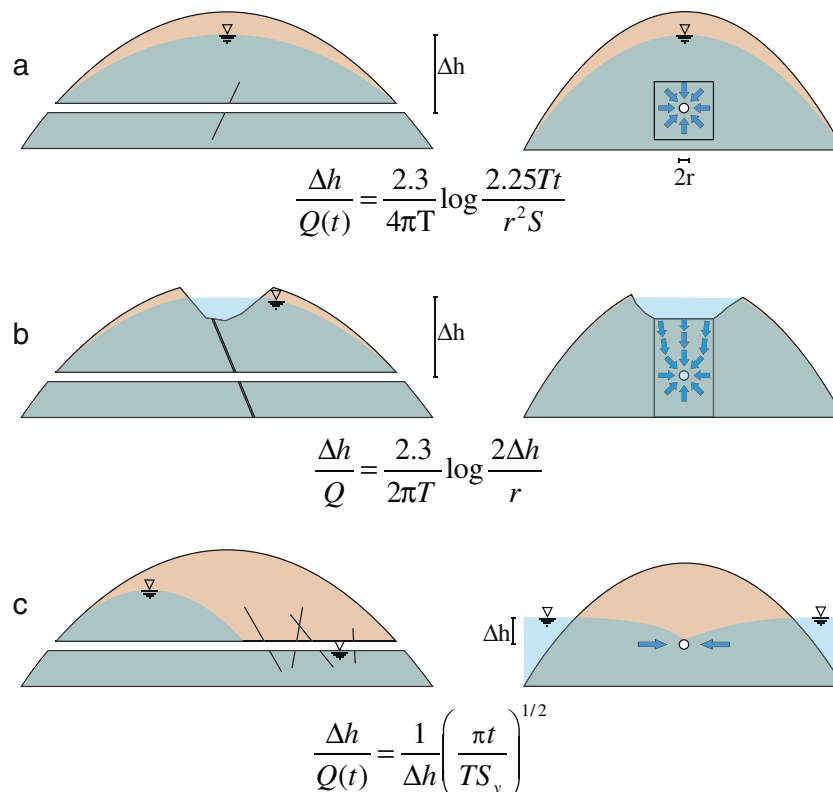

$$\frac{\Delta h}{Q(t)} = \frac{2.3}{4\pi T} \log \frac{2.25 Tt}{r^2 S}$$

$$\frac{\Delta h}{Q} = \frac{2.3}{2\pi T} \log \frac{2\Delta h}{r}$$

$$\frac{\Delta h}{Q(t)} = \frac{1}{\Delta h} \left(\frac{\pi t}{T S_y} \right)^{1/2}$$

Fig. 12 EPM (equivalent porous medium) transmissivity model sketches and formulas for **a** the radial flow without recharge transmissivity model, **b** the radial flow with constant head boundary transmissivity model, **c** the linear flow with variable water-table transmissivity model

880

This value has also been derived by other authors in similar surrounding (e.g. Maréchal et al. 2004, 2006). As an example, the third model is used to compute transmissivity for the northern shallow section of the Gas Transit Obergesteln Drift affected by toppling, resulting in open vertical fractures oriented perpendicularly to the tunnel axes.

Results

Transmissivity distribution

The transmissivity distribution for all geological units combined is plotted on the semi-logarithmic histogram in Fig. 13. The binning size is equal to one logarithmic cycle. Transmissivity values computed from both continuous flow rates (black bar) and dripping flow rates (grey bar) are represented. Transmissivity values range over 9 orders of magnitude from 10^{-10} to 10^{-1} m²/s. Figure 14 shows the distribution of transmissivity when continuous and dripping inflows are summed for every 100-m interval. The resulting transmissivity distribution could be bimodal or lognormal. The true transmissivity distribution of continuous inflows is probably close to lognormal as suggested by Fig. 15. In this figure, the transmissivity distribution derived from high-quality continuous inflow measurements of the Gotthard A2 security gallery (black line) is plotted on a double logarithmic graph of transmissivity versus cumulative number. The grey line represents a lognormal synthetic sample with the same mean, variance and data number. Figure 16 shows histograms of the transmissivity distribution of each geological unit. The binning is again logarithmic and each bin corresponds to one log cycle. Transmissivity values derived from both dripping inflows (grey bars) and continuous inflows (black bars) are represented.

Transmissivity distribution versus depth

The 100-m interval transmissivity distribution of each geological unit and of all geological units combined are plotted versus depth in Fig. 17. The data, represented by
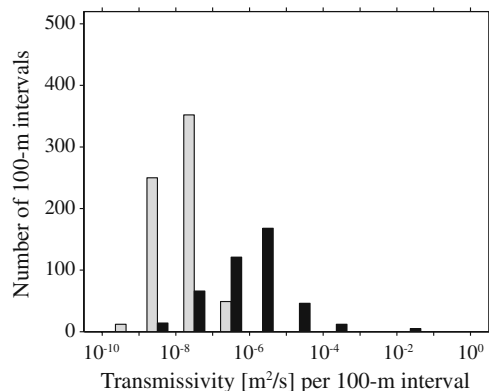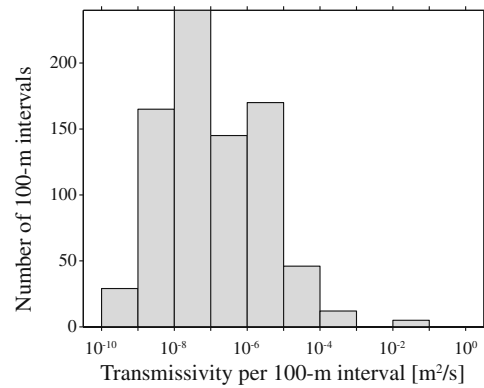

Fig. 14 Histogram showing transmissivity values derived from the dripping and continuous inflow rates for all geologic units

crosses (model 1), circles (model 2) and triangles (model 3), are plotted with arithmetic (black) and geometric (dashed grey) moving averages of 200-m-sized windows. Only transmissivities computed from continuous inflow rates are shown in this figure. Transmissivity values close to the ground surface are more scattered than at depth. This results from the difficulty to interpret and convert shallow tunnel inflow rates into transmissivity values. At depths greater than 400 m, the rock-mass is always saturated and inflows are less difficult to interpret, even after long term drainage conditions. The 100-m interval transmissivity values below 400-m depth typically range from 10^{-9} to 10^{-4} m²/s with an arithmetic and geometric mean around 10^{-6} m²/s and show no global trend with depth. The deeper transmissivity values from the ASG and GSG geological units (mainly gneisses and schists) have a weak tendency to decrease with increasing depth. The deeper AAG, GAK, GHG geological units (mainly granitic rocks) have transmissivity values which show no decreasing trend with increasing depth.

Transmissivity distribution along selected tunnels

Finally, Fig. 18 shows plots of the transmissivity distribution along selected tunnels. These tunnels have been chosen
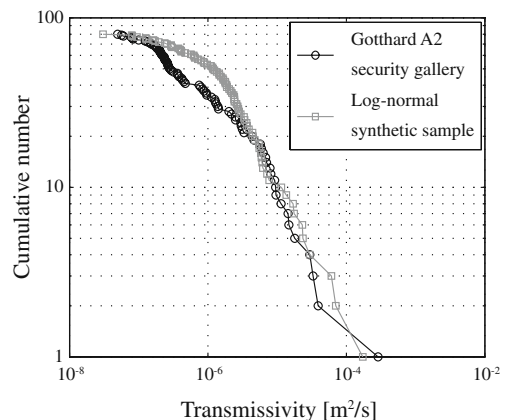

Fig. 13 Histogram showing transmissivity values derived from dripping inflow rates (*grey*) and continuous inflow rates (*black*) for all geologic units

Fig. 15 Transmissivity cumulative plot for Gotthard A2 security gallery (*black*) compared with a lognormally distributed synthetic sample of same size, mean and variance (*grey*)
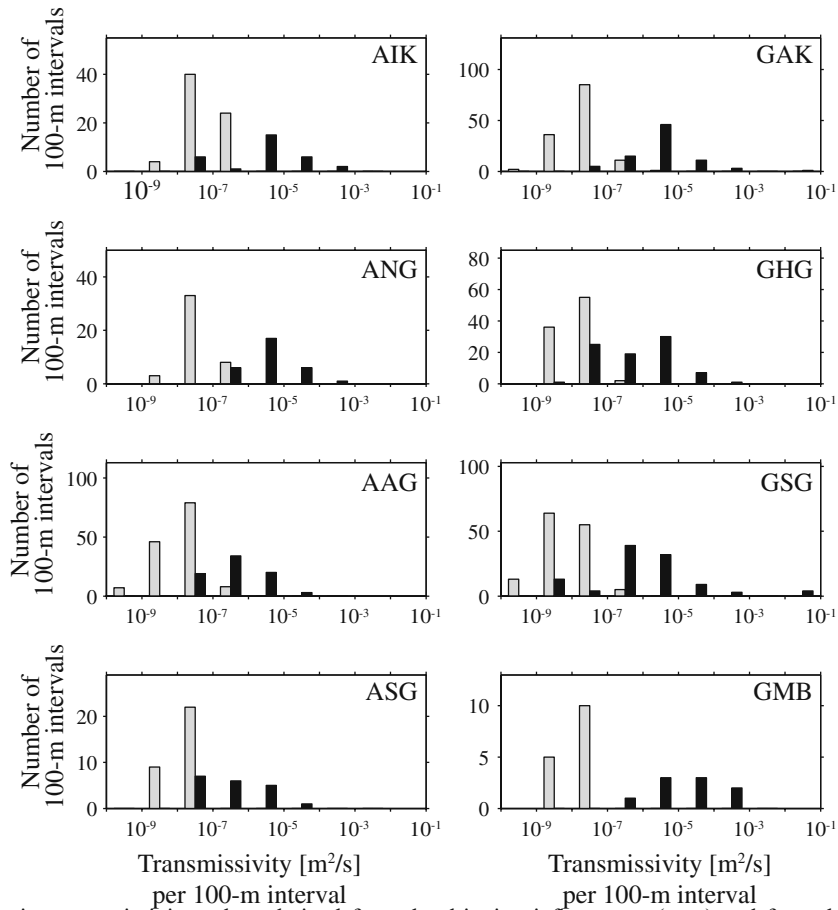
Fig. 16 Histograms showing transmissivity values derived from the dripping inflow rates (*grey*) and from the continuous inflow rates (*black*) for each geologic unit
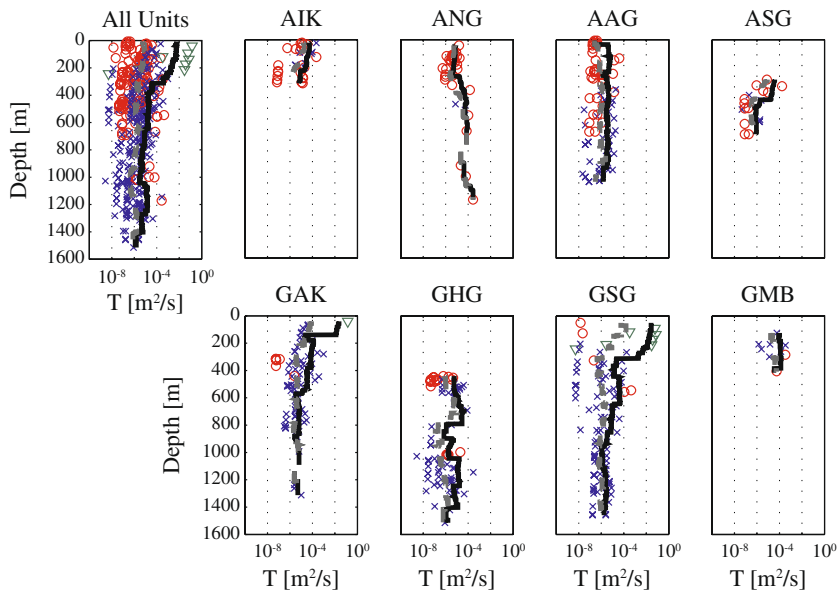

Fig. 17 Plots of the transmissivity values derived with the radial flow without recharge transmissivity model (model 1, *blue crosses*), the radial flow with constant head boundary transmissivity model (model 2, *red circles*) and the linear flow with variable water table transmissivity model (model 3, *green triangles*) versus depth with logarithmic (*dashed grey line*) and arithmetic (*black line*) moving averages (200 m) for all geologic units and for each of them
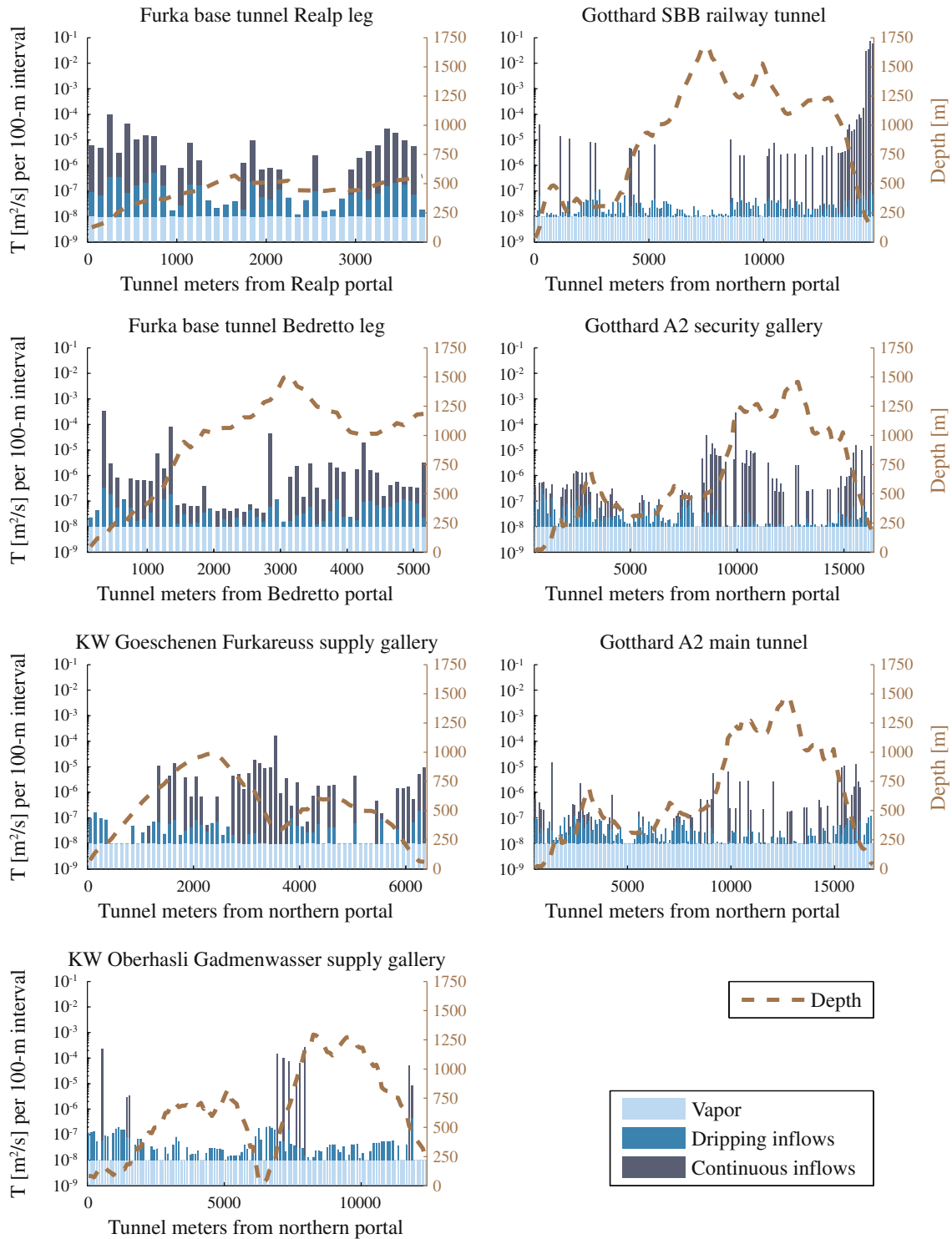
Fig. 18 Transmissivity distribution along tunnel with *dark blue bars*, representing transmissivity values derived from continuous inflow rates stacked onto *medium blue bars,* representing transmissivity values derived from dripping inflow rates, finally stacked onto *light blue bars,* representing the minimum transmissivity derived from water vapor output measurements in the Gotthard base tunnel, for selected tunnels: a, b, h, j, c, d and e (see Fig. 2 caption)

for the higher quality of their inflow data. Bars represent the total transmissivity value per 100-m interval accounting for the continuous inflows, the dripping inflows and the water vapor flow. The water vapor flow has been taken into account by assigning each 100-m interval a transmissivity value of 10^{-8} m^2/s. Again, the greatest uncertainty in the

computed transmissivities is related to the tunnel sections with shallow depth. For example, the Gotthard SBB railway tunnel in Fig. 18 indicates a highly transmissive section close to the southern portal of the Gotthard SBB tunnel. In other sections with similar geological and hydrogeological conditions (Gas Transit Obergesteln gal-

lery; Furka base tunnel Bedretto gallery), such high inflows have not been included in the main data base because they only represent early time inflows.

Rock mass effective hydraulic conductivity

Data processing and conductivity models

Different models have been used to estimate rock mass effective hydraulic conductivity from the individual inflow transmissivities (Löw et al. 1996). The equations of the three different effective hydraulic conductivity models are summarized in Fig. 19. These models are all derived from a general effective hydraulic conductivity model for fractured rocks as described for example in Voborny et al. (1994):

$$K_{eff,i} = G_i \overline{T} F \tag{2}$$

with

- $K_{eff,i}$: diagonal ii-components of the effective K-Tensor
- G_i: geometric factor describing conductive fracture orientation and extension
- $\overline{T}$: mean T-value of conductive fractures (arithmetic or geometric, see text)
- F: frequency of conductive fracture

If a single family of equidistant parallel features of infinite extent has a lognormal distribution of its transmissivity values, then the effective hydraulic conductivity in the direction of the features is proportional to the arithmetic mean of the distribution (Voborny et al. 1993, unpublished report, see Table 1). This relation is used to compute the effective vertical hydraulic conductivity. In contrast, if the extent of the features is limited, the orientation of the

$$K_{eff,vertical} = \overline{T} F$$

$$K_{eff,isotropic} = \frac{2}{3} \overline{T} 2F$$

$$K_{M,isotropic} = \frac{2}{3} \overline{T} 2F$$

Fig. 19 EPM hydraulic conductivity model sketches and formulas for **a** the vertical fracture hydraulic conductivity model, **b** the isotropic fracture hydraulic conductivity model and **c** the isotropic matrix hydraulic conductivity model

features is isotropic, their spatial distribution is homogeneous and their transmissivities are lognormally distributed, then the effective hydraulic conductivity is proportional to the geometric mean of the distribution (Gelhar 1987).

All three models used are strong simplifications and assume that matrix conductivity is negligible (no leakage) and conductive fractures have homogeneous transmissivity (no channeling). The first two models refer to the bulk rock mass hydraulic conductivity from sets of fractures feeding continuous inflows. The third model represents hydraulic conductivity from sets of fractures feeding dripping inflows. The main difference between models 2 and 3 and model 1 is the assumed distribution of fracture orientations (isotropic versus vertical): models 2 and 3 can be viewed as representing intermediate and small-scale fractures (joints) which show a nearly isotropic distribution of spatial orientation, and model 1 as representing the larger-scale faults, striking at a large angle to the tunnel axes and dipping steeply towards the south or north. Whereas models 2 and 3 give isotropic hydraulic conductivity, model 1 only considers vertical hydraulic conductivity. Because all available data refer to 100-m-interval transmissivity and not individual fracture transmissivity, frequencies and transmissivity means are referred to 100-m tunnel intervals with continuous inflows (models 1 and 2) or dripping inflows (model 3).

Results

Figure 20 shows plots of the distribution of the effective hydraulic conductivity as a function of depth for the three effective hydraulic conductivity models. From the analysis of the plots for all geological units combined one can conclude that:

- The uppermost 200–400 m below ground surface show strongly increased hydraulic conductivities.
- Below this section, the fracture-related isotropic effective hydraulic conductivity, as well as the matrix isotropic effective hydraulic conductivity, remains constant with increasing depth.
- Below 200–400 m, the fault zone-related vertical effective hydraulic conductivity weekly decreases with increasing depth.

Concerning the individual geologic unit plots:

- Below the near surface unloading section, a decrease of the effective hydraulic conductivity is observed in gneissic and schistose rocks of ASG, GSG and GAK.
- Both granitic units (AAG and GHG) show no clear trend of the effective hydraulic conductivity with increasing depth. The large scatter in the GHG profile results from localized occurrence of highly conductive brittle faults. Such faults have not been encountered in tunnel sections crossing the AAG unit.
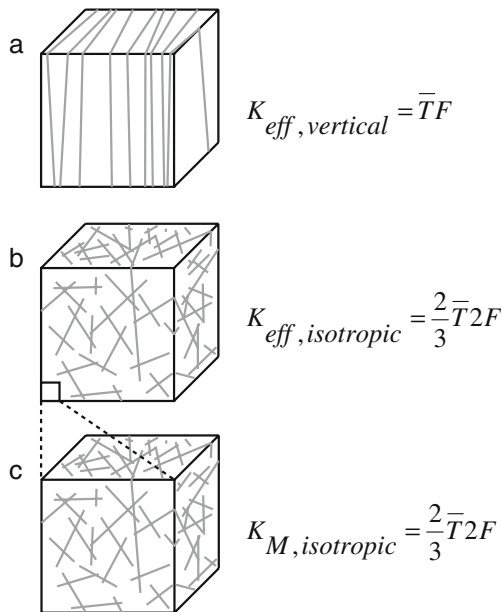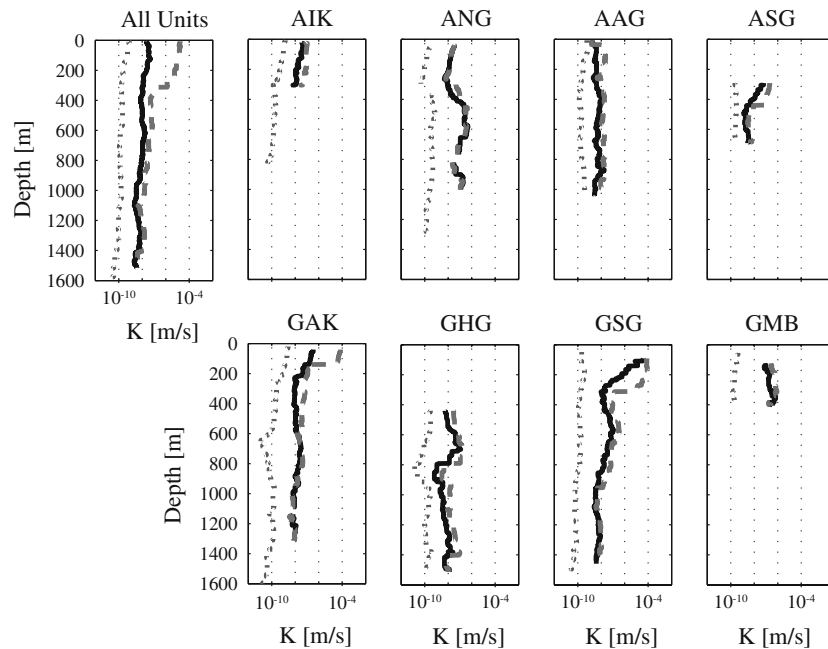
Fig. 20 Plots of the hydraulic conductivity values derived with the isotropic fracture hydraulic conductivity model (*black line*), the vertical fracture hydraulic conductivity model (*dashed grey line*) and the isotropic matrix hydraulic conductivity model (*dotted grey line*) for all geologic units and for each of them

Discussion

In this section, the inflow spatial variability, some of the critical model assumptions for transmissivity and hydraulic conductivity estimations, and the resulting transmissivity and effective hydraulic conductivity distributions are interpreted and discussed. Finally the results are compared with those from other studies.

Tunnel inflow distribution and variability
The main parameter governing tunnel inflow rate is the degree of brittle tectonic overprint; the inflow rate variability due to the presence or absence of brittle tectonic features is higher than the variability due to changes in lithology or depth (see section Depth and lithology). The mean inflow rate is highly dependent on the extreme rate values which are mostly linked to important fault or fracture zones (see section Exceptionally high tunnel inflow rates). Unfortunately information concerning the type of fracture related to each inflow is not available for most of the tunnels and galleries considered. The spacing distribution of inflows (see section Inflow spacing distribution along tunnels) shows that continuous inflows, in contrast to dripping zones, are not evenly spaced and therefore difficult to predict. This unpredictability increases with the rate because high rate inflows (>10 l/s) are rare. Even if strong inflows can be related to important fault zones, locating these features does not ensure a good inflow prediction due to variations of fault architecture and channeling (only a small portion of faults are highly conductive and directly intersected by a tunnel).

Regional investigations show, that the Gotthard massif suffered much stronger brittle tectonic deformations than the Aar massif and that brittle faults of substantial width occur frequently in the Gotthard massif but not in the Aar massif (Laws 2001; Lützenkirchen 2002; Zangerl et al. 2006). With the exception of an extreme inflow from a brittle fault in the Goeschenen Voralpreuss supply gallery, granites in the Aar massif (AAG) show low inflow rates and sparse inflows with only minor influences of brittle faulting visible by the small scatter of the depth dependant inflows (Fig. 8). This is the only case where a systematic increase of tunnel inflow with depth can be observed in the first 1,000 m. The derived interval transmissivities and hydraulic conductivities are constant (Figs. 17 and 20) and indicate that in these granites inflow rates are mainly controlled by the tunnel-induced hydraulic head gradients increasing with depth.

Uncertainties in transmissivity and hydraulic conductivity estimations
The most critical assumptions of the models used to estimate fracture transmissivity (transmissivity of 100-m intervals with flowing fractures) are:

- The fracture extension is big enough to be considered as infinite or well interconnected and no leakage takes place between the fracture and the embedding matrix. However, in the long term, fluid exchange between fracture and matrix might be considerable. As most of the inflows considered here are relatively late (a few weeks), the error related to this assumption might be significant. As flow at late times should be controlled by matrix leakage, the real transmissivity values might be slightly underestimated.

– Flow in fractures is governed by Darcy's law. Because of the extremely high head gradients around open deep tunnels, non-linear turbulent flow is suspected to impact strong inflows. This process will lead to an underestimation of the true fracture transmissivity.

– Fracture apertures do not change in response to tunnel drainage. Rutqvist and Stephansson (2003) state that if stress and stiffness are high, additional closure resulting from the fluid pressure release will be insignificant at a large scale. However, significant differences between inflows to predrillings and (upscaled) inflows to tunnels at the same locations have been observed in many projects, suggesting an influence of the pore pressure and effective stress on fracture apertures around tunnels. For a depth of 500 m in granite, Ivars (2006) has carried out a detailed modeling study on the influence of hydro-mechanical coupling in fractured rock masses. He concludes that even a small change in aperture at the large depth considered has a significant effect on flow. The effect is dependant on the fractures' orientation, normal and shear stiffnesses, and friction and dilation angles. Normal stiffnesses on joints in granitic rocks have recently been compiled from laboratory tests, reported by Zangerl et al. (2008c), who applied them in a large-scale rock mass consolidation study (Zangerl et al. 2008a, b). Closure and shear of joints and faults around Alpine tunnels in response to drainage and pore pressure drawdown is shown to be significant and the cause of surface settlements amounting to about 4 cm (Zangerl et al. 2008b). For these reasons, it has to be assumed that the estimated fracture transmissivities have the tendency to underestimate the values under natural pore pressure conditions.

In summary, all assumptions made for the transmissivity derivation could have lead to a slight underestimation of the true fracture transmissivity. To compare the uncertainty of the reported transmissivity values resulting from the three different flow models, a probability density function has been assumed for each parameter included in the three different models (Fig. 12). Rate, specific storage and yield are assumed to be lognormally distributed, whereas radius, time, depth and drawdown, are assumed to be distributed normally. The probability density function of transmissivity, derived by Monte Carlo analysis, has then been computed for each selected 100-m interval based on the assumed parameter distributions and on standard deviations. Two parameter scenarios have been investigated: a "best guess" that assumes relatively small parameter standard deviations and a "worst case" with upper bound parameter standard deviations (Table 10). Specific storage is poorly known, assumed to be constant and equal to 10^{-6} 1/m (Löw et al. 1996). For this reason, this parameter has been given the highest standard deviation (10^{-5} 1/m).

The resulting transmissivity histograms for three selected 100-m tunnel intervals (one per transmissivity model) and for each scenario are plotted in Fig. 21. For the best guess parameter distributions, the Jacob and

Lohman and the constant head boundary models result in transmissivity values which are lognormally distributed and remain within one log cycle. This uncertainty of the estimated values is acceptable especially when compared to the uncertainties resulting from other types of large-scale transmissivity estimation. In contrast, the distribution resulting from the linear flow model spreads over five orders of magnitude. This high variability is related to the head gradient which is raised to the power of four in the linear flow transmissivity equation. For the worst case, the uncertainty in transmissivity for all transmissivity models is only slightly increased. Consequently one can be confident in the transmissivity values derived from the two radial flow models, and relatively cautious with the transmissivity values derived with the linear flow transmissivity model. This is confirmed by the large transmissivity variations resulting from the linear flow model as shown in Fig. 17 (triangles). The uncertainties in the hydraulic conductivity models result from some of their strong and unverified assumptions such as infinite extent of homogeneous parallel planes for the vertical fracture model or the homogeneous distribution and interconnectivity of conductive fractures for both isotropic models.

Transmissivity and effective hydraulic conductivity distribution

As shown in Fig. 13, the shape of both dripping and continuous inflow transmissivity distributions is close to the shape of a lognormal distribution, whereas in Fig. 14, when both types of transmissivity values are summed over each 100-m interval, the resulting distribution looks bimodal and skewed. This bimodal aspect could result from an incomplete sampling of continuous inflow rates lower than 0.01 l/s or from an underestimation of the dripping rates. If it reflects reality, then it implies that continuous inflows and dripping zones are issued from different fracture systems. This explanation would support the conceptual model hypothesis that dripping inflows are related to a small fracture network belonging to the matrix, whereas continuous inflows are often related to a bigger network of faults.

The effective hydraulic conductivity distribution of all geological units combined (Fig. 20), is about 10^{-8} m/s for the isotropically oriented fracture model, ranges from 10^{-8} to 10^{-5} m/s for the vertical fault zone model and is about 10^{-10} m/s for the matrix model. Again, the unloading zone in the uppermost 200–400 m is clearly visible, both in the combined plot and in the individual foliated rock units (toppling can not occur in granites because they lack a steeply dipping foliation set).

Concerning the individual geologic unit plots, a decrease of the effective hydraulic conductivity with depths below the unloading zone is weakly expressed in gneisses and schists of ASG and GSG. For all other geologic units, effective hydraulic conductivity remains more or less constant with increasing depth. The presence of a decrease in the hydraulic conductivity for some gneisses and schists with increasing depth can be

Table 10 Monte Carlo simulation of transmissivity distribution

Geologic unit	AIK				GSG	
Tunnel	KW Oberhasli Gadmenwasser				Gotthard SBB	
Interval middle location [Tm]	550		1,450		14,450	
Transmissivity model	Model 2		Model 1		Model 3	
Depth [m]	127		185		213	
Assumed depth SD [m]	25	100	25	100	25	100
Continuous inflow rate [l/s]	40.0	40.0	0.5	0.5	29.3	29.3
Assumed rate SD [l/s]	20	20	0.25	0.25	87.9	87.9
Elapsed time	3 w	3 w	3 w	3 w	1.2 y	1.2 y
Elapsed time SD	0.6 w	1.5 w	0.6 w	1.5 w	0.25 y	0.6 y
Storativity [-]	10^{-6}	10^{-6}	10^{-6}	10^{-6}	10^{-6}	10^{-6}
Storativity std [-]	10^{-5}	2×10^{-5}	10^{-5}	2×10^{-5}	10^{-5}	2×10^{-5}
Specific yield [-]	0.01	0.01	0.01	0.01	0.01	0.01
Specific yield std [-]	0.02	0.05	0.02	0.05	0.02	0.05
Tunnel radius [m]	3	3	3	3	4	4
Tunnel radius std [m]	0.3	0.6	0.3	0.6	0.4	0.8
Drawdown [m]	127	127	185	185	134.5	134.5
Drawdown SD [m]	25.4	63.5	37	95.5	26.9	67.25

SD standard deviation; *w* weeks; *y* years

explained by the lower stiffness of fractures and faults in gneisses and schists compared to granitic rocks. As shown by Laws et al. (2003) fractured zones in gneisses (damage zones with cm-spaced fractures with 1-mm infill and microfractures) of the Aar Massif have tangent Young's moduli (at 5 MPa confining pressure) ranging between 0.05–1.3 GPa, whereas the same zones in granites show values ranging between 1.5 and 14 GPa. At the same confining pressure of 5 MPa, the ratio of stiffness of the fault core (cohesionless microbreccia) in granite and the stiffness of the fault core in gneiss is about 3. This implies that, at least at shallow depth, gneisses and schists have a stronger response to changes in effective stress (Laws et al. 2003). For brittle faults with thick infillings of cataclastic materials, the relationships between stress and permeability as derived for porous media might be applicable—as in, for example, the Kozeny-Carman equation. For smooth parallel plate joints, the cubic law relates aperture change to permeability. Both relationships imply a strong non-linearity between porosity change and permeability. Therefore, stiffer fault rocks at greater depth (see Laws et al. 2003) might still show depth-dependant transmissivity.

Comparison with other studies

Systematic analyses of tunnel inflows have also been carried out in other regions (e.g. Cesano et al. (2000; Gargini et al. 2008). Cesano et al. (2000) showed that the thickness and composition of the weathered material and unconsolidated deposits above the intact bedrock surface were important factors in regulating groundwater inflows to the Bolmen tunnel (Sweden). The Bolmen tunnel's depth varies between 30 and 90 m, whereas in the present study, in Switzerland most of the inflows considered come from bigger depths. For shallow flow systems, the effects of surface deposits on groundwater recharge and tunnel inflow are much more pronounced. As shown by spring observations and numerical modeling (e.g. Loew et al.
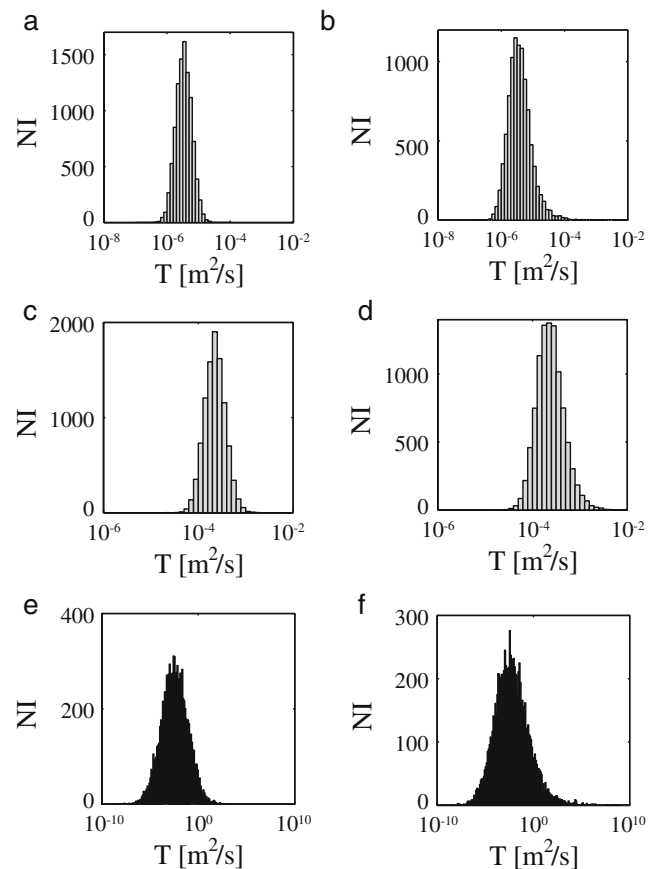

Fig. 21 Plots of simulated transmissivity distributions for: **a** the 1,400–1,500-m interval of KW Oberhasli Gadmenwasser supply gallery (radial flow without recharge transmissivity model) with best-guess parameter standard deviations; **b** the same interval with worst-case parameter standard deviations; **c** the interval 500–600 m of the same gallery (radial flow with constant head boundary transmissivity model) with best-guess parameter standard deviations and; **d** the same interval with worst-case parameter standard deviations; **e** the 14,400–14,500-m interval of Gotthard SBB railway tunnel (linear flow transmissivity model) with best-guess parameter standard deviations; **f** the same interval with worst-case parameter standard deviations

2007; Ofterdinger 2001) the interactions between the water table and the draining tunnel are of minor importance for deep Alpine tunnels.

Gargini et al. (2008) integrated a large amount of spring and tunnel inflow data in the Northern Apennines and identified three distinct and hierarchically nested groundwater-flow systems. The shallowest (150–200 m deep) and most permeable was hosted by the detensioned portion of the rock mass. A second flow system reaching 300–400 m depth, and a third flow system of up to 2,000 m depth were related to tectonic faults. In comparison to observations for this Swiss study, the first flow system type can be confirmed. Because of the stronger relief, the depth of the mass movement and unloading phenomena is deeper in the Swiss study area (Klemenz 1974, Loew et al. 2007).

The published transmissivity and effective hydraulic conductivity values of crystalline rocks are mainly derived from borehole packer tests (Mazurek 1993; Stober 1997). When comparing transmissivity or permeability values obtained from tunnel inflow data with transmissivity or effective hydraulic conductivity values derived from packer tests, it is important to note that the volume tested by a deep tunnel is much bigger than that of a surface-based borehole hydrotest. This is due to the large pressure drawdown induced by an open deep tunnel, the drawdown duration and the dimensions of the excavation. This might influence the comparison of hydraulic conductivity if this property is indeed scale-dependent as suggested for example by Brace (1980) and Clauser (1992).

The deepest inflow (1.2 l/s) included in the full data set was reported from the Bedretto gallery at a depth of 1,515 m. The existence of high inflows into underground excavations in crystalline rocks of that depth is not surprising. In the French part of Mont Blanc tunnel (linking France to Italy), for example, a cumulate inflow rate of 140 l/s was measured along a 750-m section whose depth is greater than or equal to 2,000 m (Gudefin 1967). Moreover, the existence of deep water circulation in crystalline rocks has been demonstrated in several deep boreholes. For example, in a hot dry rock (HDR) well in Urach, Germany, water circulation in an open fracture system has been detected by hydraulic tests at depths of 3 −4 km (Stober and Bucher 1999).

An extensive review and a discussion of deep borehole hydraulic test results from crystalline rocks can be found in Stober and Bucher (2007). The range of hydraulic conductivity values derived for granites in the present study ($K=10^{-11}-10^{-7}$ m/s) is on the lower side of the range of hydraulic conductivity values reported for similar rocks ($K=10^{-11}-10^{-4}$ m/s) and the range of hydraulic conductivity values for gneisses in this study ($K=10^{-11}-10^{-4}$ m/s) is quite similar to the range of hydraulic conductivity values derived from deep boreholes of northern Switzerland ($K=10^{-13}-10^{-4}$ m/s). Despite the fact that hydraulic conductivity values derived by inflow analysis are representative for larger volumes of rock than packer tests, the hydraulic conductivity values derived from both methods are comparable.

According to Stober and Bucher (1999), granites of the Black Forest (Germany) are on average more permeable than gneisses. This difference is attributed to differences in texture and mineral composition which in turn causes granites to deform in a more brittle fashion than gneisses. Stober (1995; 1997) also reports that, in the Black Forest, a general permeability decrease with depth characterizes the gneisses but not the granites. Both trends can also be identified in the data set reported in this paper.

Summary and conclusions

In the central Aar and Gotthard massifs (Switzerland), groundwater inflows to 136 km of tunnels and galleries have been analyzed in order to characterize the hydraulic properties of different geological units and investigate their dependency on different parameters like depth, lithology and tectonic faulting. Inflow rates per 100 m of tunnel are converted into transmissivity values by means of basic transmissivity models like the Jacob and Lohman approximation for radial flow to a well with constant drawdown. Transmissivity values are then converted into hydraulic conductivity values with analytical equivalent porous medium (EPM) models.

The distribution of inflow frequency and rate can be described by two main depth intervals. The first interval ranges from the surface down to 200–400 m of depth. In most of the geological units (ANG, AAG, GHG, GMB), this interval is characterized by a low inflow frequency and rate, both of which increase with depth. Exceptions are AIK, GAK and GSG geological units which exhibit relatively high frequencies and rates from the surface. The authors interpret this interval to be a variably saturated zone of enhanced permeability resulting from stress release and slope deformation phenomena. Stress release and slope deformations (often related to deep toppling) can open joints and induce very high, large effective hydraulic conductivities. Given the Alpine topography, the inflows in these near surface sections can be low because of deep water tables (tunnel sections can be above the water table initially or after short term drainage). Therefore, close to the surface (up to 200–400 m) the spatial distribution of groundwater flow depends on:

– Topography: steep slopes in hard rocks are more susceptible to unloading phenomena and gravitational movements than moderate hill slopes
– Valley orientation with respect to the foliation: toppling occurs when the steeply dipping foliation runs parallel to the valley axes
– Rock fabric: rocks presenting no foliation (granites or massive gneisses) are not affected by toppling but can develop exfoliation fractures parallel to the topography that decrease in frequency and persistence with depth

Below 200–400 m depth, increasing (AAG) and decreasing (ASG, GAK, GSG) trends of inflow rates are observed, as long as they are not superimposed by a few

strong inflows from brittle fault zones. These differences in trends are related to the variations in stiffness of fractured gneisses and granites—as shown by lab experiments on cores from the Aar massif at 5 MPa confining pressure, the stiffness of fractured zones (damage zones) in gneisses is about one order of magnitude smaller than in granites. The authors suggest that the stiffness of fractured granites is so low, that in the upper 400–1,500 m, increasing effective stresses with depth has no measurable effect on fracture apertures and permeability. On the other hand, the induced hydraulic head gradients around tunnels that increase with depths lead to slightly increasing inflow rates in this depth interval. The low stiffness of fractured rocks in gneisses and schists significantly reduces fractures apertures and transmissivity in the observed depth range of up to 1,500 m.

Below 200–400-m-depth brittle faulting is the dominant parameter controlling inflow frequency and rate. The study shows that significant regional variations in brittle tectonic overprint exist. Mainly ductile Alpine deformation structures (fine grained metamorphic mylonites) are found in the Aar massif shear zones, whereas in the Gotthard massif, most ductile Alpine shear zones have been strongly reactivated under brittle conditions. The more intensive brittle tectonic overprint of the Gotthard massif clearly translates into a higher mean tunnel inflow rate compared to the Aar massif.

The spacing distribution of inflows along tunnels or galleries is a function of the inflow rate. Low rate inflows (dripping zones) follow a negative exponential distribution and are more evenly distributed and more abundant than higher-rate inflows (continuous inflows) which follow power law distributions and appear in clusters. Inflows with outstanding rates are rare and unpredictable. However, these rare and extreme inflows have a big impact on the total flow into an underground excavation. Whereas in the entire study area, the mean inflow rate per 100-m tunnel segment is about 2 l/s; more than 90% of the total flow rate is fed by intervals whose rate is bigger or equal to 1 l/s.

Transmissivity distribution has been derived from the fracture inflows to 100-m-long tunnel segments using three types of analytical flow models, frequently used in the analysis of tunnel inflows. These models rely on important assumptions regarding fracture persistence, leakage, laminar flow and hydro-mechanical coupling. It is shown that the analytical equations used have the tendency to underestimate the undisturbed fracture transmissivities.

Down to 200–400 m depth, transmissivity values per 100 m of tunnel (10^{-9}–10^{-1} m^2/s) are higher on average and are more scattered than at larger depths (10^{-5}–10^{-4} m^2/s). The higher transmissivity is a real characteristic of the shallower part of the rock mass, whereas the higher scatter of the data could be partially an artifact resulting from the difficulty to interpret and convert shallow tunnel inflow rates into transmissivity values. The transmissivity values tend to decrease in the gneissic or schistous geological units (ASG, GSG), whereas no

trend is observed for the granitic units (AAG, GAK, GHG). The transmissivity distribution of continuous inflows is close to a lognormal distribution.

As equivalent porous medium (EPM) hydraulic conductivities are computed with mean transmissivities, they essentially show the same characteristics. A more permeable zone at shallow depths (up to 200–400 m) is characterized by values ranging between 10^{-10} and 10^{-4} m/s. A deeper zone of constant (AAG, GHG) or decreasing (ASG, GSG, GAK) hydraulic conductivity shows values ranging between 10^{-10} and 10^{-7} m/s. The decrease in EPM hydraulic conductivity is again related to effective stress dependant closure of fractures in gneissic rocks or schists. Strong deviations from these trends are related to brittle faults that appear as important preferential groundwater pathways, also at great depth.

Appendix 1: Notation

$A[m^3/s]$	Air flow rate at airway entrance
$C[]$	Channeling factor
$c_1[kg/kg]$	Air water content at the first measuring point 1
$c_2[kg/kg]$	Air water content at the first measuring point 2
$F[m^{-1}]$	Frequency of the water conducting structures
$G_i[]$	Geometrical factor
$h[m]$	Hydraulic head
$K[m/s]$	EPM hydraulic conductivity
$K_{eff,i}[m/s]$	Diagonal components of the effective hydraulic conductivity tensor
$K_M[m/s]$	Matrix hydraulic conductivity
$L[m]$	Tunnel length
$m[kg/s]$	Water vapor mass flow rate
$P[Pa]$	Absolute air pressure
$P_w[Pa]$	Water vapor partial pressure
$Q[m^3/s]$	Flow rate
$r[m]$	Tunnel radius
$R_f\ [J/(kg \times K)]$	Gas constant for wet air
$R_L[J/(kg \times K)] = 287.1$	Gas constant for air
$S[]$	Storativity
$S[1/m]$	Specific storage
$S_y[]$	Specific yield
$T[m^2/s]$	Transmissivity
$\overline{T}[m^2/s]$	Mean transmissivity
$t[s]$	Time elapsed
Temp$[K]$	Dry bulb temperature
$V[l/s]$	Water vapor volumetric flow rate

V_2[l/s/m]	Water vapor volumetric flow rate per meter
V_3[l/s/hm]	Water vapor volumetric flow rate per hectometer
Δc[kg/kg]	Airway water vapor content
Δh[m]	Drawdown
ρ[kg/m^3]	Air density

Appendix 2: Water vapor flow rate derivation according to the Ideal Gas Law

$$R_f = R_L \frac{1}{1 - 0.378 \frac{P_w}{P}} \tag{3}$$

$$\rho = \frac{P}{R_f \times Temp} \tag{4}$$

$$m = A \times \rho \tag{5}$$

$$\Delta c = c_2 - c_1 \tag{6}$$

$$V = m \times \Delta c \tag{7}$$

$$V_2 = V/L \tag{8}$$

$$V_3 = 100 V_2 \tag{9}$$

References

Abrecht J (1994) Geologic units of the Aar massif and their pre-Alpine rock associations: a critical review. Schweiz Mineral Petrogr Mitt 74:5–27

Brace WF (1980) Permeability of crystalline and argillaceous rocks. Int J Rock Mech Min Sci Geomech Abstr 17:241–251

Bucher S (2006) Talklüfte im östlichen Aarmassiv (Schöllenen-Schlucht) [Exfoliation joints in the eastern Aar massif]. Diploma Thesis, ETHZ, Switzerland

Cacas MC, Ledoux E, Marsilly GD, Tillie B, Barbreau A, Durand E, Feuga B, Peaudecerf P (1990) Modeling fracture flow with a stochastic discrete fracture network: calibration and validation 1 —the flow model. Water Resour Res 26:479–489

Cesano D, Olofsson B, Bagtzoglou AC (2000) Parameters regulating groundwater inflows into hard rock tunnels: a statistical study of the Bolmen Tunnel in Southern Sweden. Tunn Undergr Space Technol 15:153–165

Choukroune P, Gapais D (1983) Strain pattern in the Aar Granite (Central Alps): orthogneiss developed by bulk inhomogeneous flattening. J Struct Geol 5:411–418

Clauser C (1992) Scale effects of permeability and thermal methods as constraints for regional-scale averages. In: Quintard M, Todorovic M (eds) Heat and mass transfer in porous media. Elsevier, Amsterdam

Davy P, Bour O, De Dreuzy J-R, Darcel C (2006) Flow in multiscale fractal fracture networks. In: Cello G, Malamud BD (eds) Fractal analysis for natural hazards. Geological Society, London

Doe TW (1991) Fractional dimension analysis of constant-pressure well tests. SPE paper 22702, Society of Petroleum Engineers, Richardson, TX

Eckart P, Funk H, Labhart TP (1983) Postglaziale Krustenbewegung an der Rhein-Rhone-Linie [Post-glacial crustal movements along the Rhine-Rhone line]. Vermess Photogr Kulturtech 2:83

El Tani M (1999) Water inflow into tunnels. In: Alten T, Backer L, Bollingmo P, Broch E, Holmoy K, Holter KG, Nielsen K (eds) World Tunnel Congress 1999 on Challenges for the 21st Century, Oslo, Norway, 29 May–3 June 1999

Frei B, Breitenmoser T (2006) Geologisch-geotechische und hydrogeologische Verhältnisse im Vortrieb Amsteg: Vergleich zwischen Prognose und Befund [Geological, geotechnical and hydrogeological settings of the Amsteg section: comparison of prediction and on-site findings]. In: Löw S (ed) Geologie und Geotechnik der Basistunnels am Gotthard und am Lötschberg. Hochschulverlag, Zürich

Frei B, Löw S (2001) Struktur und Hydraulik der Störzonen im südlichen Aar-Massiv bei Sedrun [Structure and hydraulic properties of shearzones of the southern Aar massif in the vicinity of Sedrun]. Eclogae Geol Helv 94:13–28

Frey M, Bucher K, Frank E, Mullis J (1980) Alpine metamorphism along the geotraverse Basel-Chiasso: a review. Eclogae Geol Helv 73:527–546

Gargini A, Vincenzi V, Piccinini L, Zuppi G, Canuti P (2008) Groundwater flow systems in turbidies of the Northern Apennines (Italy): natural discharge and high speed railway tunnel drainage. Hydrogeol J 16:1577–1599

Gelhar LW (1987) Applications of Stochastic models to solute transport in fractured rocks. Technical Report SKB, SKB, Stockholm

Goodman RE, Moye DG, Schalkwyk AV, Javandel I (1965) Ground water inflows during tunnel driving. Bull Assoc Eng Geol 2:39–56

Gudefin H (1967) Observations sur les venues d'eau au cours du percement du tunnel sous le Mont-Blanc [Findings related to inflows during the excavation of Mont Blanc tunnel]. Bull BRGM 4:95–107

Herwegh M, Pfiffner OA (1999) Die Gesteine der Piora-Zone (Gotthard-Basistunnel) [Rocks of the Piora zone (Gotthard base tunnel)]. In: Loew S, Wyss R (eds) Vorerkundung und Prognose der Basistunnel am Gotthard und am Lötschberg. Balkema, Rotterdam, The Netherlands

Hwang J-H, Lu C-C (2007) A semi-analytical method for analyzing the tunnel water inflow. Tunn Undergr Space Technol 22:39–46

Ivars DM (2006) Water inflow into excavations in fractured rock: a three-dimensional hydro-mechanical numerical study. Int J Rock Mech Min Sci 43:705–725

Jacob CE, Lohman SW (1952) Nonsteady flow to a well of constant drawdown in an extensive aquifer. Trans Am Geophys Union 33

Keller F, Schneider TR (1982) Der Furka Basis-Tunnel: Geologie und Geotechnik [The Furka base tunnel: geology and geotechnics]. Schweizer Ing Architekt 100:512–520

Keller F, Wanner H, Schneider TR (1987) Geologischer Schlussbericht Gotthard-Strassentunnel, Zusammenfassung [Final geological report of the Gotthard highway tunnel]. Beiträge Geol Schweiz Geotech Serie 70:1–67

Klemenz W (1974) Die Hydrogeologie des Gebirges im Obergestelnstollen [Hydrogeology of the rock mass in Obergesteln gallery]. Gas-Wasser-Abwasser 54:287–289

Kohl T, Signorelli S, Rybach L (2000) Constraints on Palaeo-topography by revised Apatite FT uplift rates, 25 April 2000, EGS 25th Gen. Assembly, Nice, France

Labhart TP (1977) Aarmassiv und Gotthardmassiv [Aar and Gotthard massifs]. Borntraeger, Berlin

Labhart TP (1999) Aarmassiv, Gotthardmassiv und Tavetscher Zwischenmassiv: Aufbau und Entstehungsgeschichte [Aar, Gotthard and Tavetsch massifs: structure and history]. In: Loew S, Wyss R (eds) Vorerkundung und Prognose der Basistunnels am Gotthard und am Lötschberg, Balkema, Rotterdam, pp 31–34

Laws S (2001) Structural, geomechanical and petrophysical properties of shear zones in the Eastern Aar Massif, Switzerland. PhD Thesis, ETHZ, Switzerland

Laws S, Loew S, Eberhardt E (2000) Structural make-up and geophysical properties of brittle fault zones in the eastern Aar

Massif, Switzerland. International Conference on Geotechnical and Geological Engineering, Melbourne, Australia, November 2000

Laws S, Eberhardt E, Loew S, Descoeudres F (2003) Geomechanical properties of shear zones in the Eastern Aar Massif, Switzerland and their implication on tunneling. Rock Mech Rock Eng 36:271–303

Lei S (1999) An analytical solution for steady flow into a tunnel. Ground Water 37:23–26

Lei S (2000) Steady flow into a tunnel with a constant pressure head. Ground Water 38:643–644

Loew S (2001) Natural groundwater pathways and models for regional groundwater flow in crystalline rocks. In: Seiler KP, Wohnlich S (eds) New approaches characterizing groundwater flow (Proceedings of the XXXI IAH Congress), Munich, Germany, September 2001

Loew S (2002) Groundwater hydraulics and environmental impacts of tunnels in crystalline rocks. Paper presented at the IAEG, Durban, South Africa, December 2002

Loew S, Ziegler H-J, Keller F (2000) Alptransit: engineering geology of the longest tunnel system. GeoEng2000, Melbourne, December 2000, Technomic, Melbourne, Australia

Loew S, Luetzenkirchen VH, Ofterdinger US, Zangerl C, Eberhardt E, Evans KF (2007) Environmental impacts of tunnels in fractured crystalline rocks of the Central Alps. In: Krasny J, Sharp JM (eds) Groundwater in fractured rocks. Selected Papers 9, IAH, Goring, UK, pp 507–526

Long JCS, Karasaki K, Davey A, Peterson J, Landsfeld M, Kemeny J, Martel S (1991) An inverse approach to the construction of fracture hydrology models conditioned by geophysical data an example from the validation exercises at the Stripa mine. Int J Rock Mech Min Sci Geomech Abstr 28:121–142

Löw S, Ehrminger B, Klemenz W, Gilby D (1996) Abschätzung von Bergwasserzuflüssen und Oberflächenauswirkungen am Beispiel des Gotthard-Basistunnel [Estimation of tunnel inflows and surface effects using the example of Gotthard base tunnel]. In: Oddson B (ed) Instabile Hänge und andere risikorelevante natürliche Prozesse, Birkhauser, Basel, Switzerland

Lützenkirchen VH (2002) Structural geology and hydrogeology of brittle fault zones in the Central and Eastern Gotthard Massif, Switzerland. PhD Thesis, ETHZ, Switzerland

Maréchal JC, Dewandel B, Subrahmanyam K (2004) Use of hydraulic tests at different scales to characterize fracture network properties in the weathered-fractured layer of a hard rock aquifer. Water Resour Res 40. doi:10.1029/2004wr003137

Maréchal JC, Dewandel B, Ahmed S, Galeazzi L, Zaidi FK (2006) Combined estimation of specific yield and natural recharge in a semi-arid groundwater basin with irrigated agriculture. J Hydrol 329:281–293

Marquer PD (1990) Structures et déformation alpine dans les granites hercyniens du massif du Gotthard (Alpes centrales suisses) [Alpine structures and deformation in the Hercynian granites of the Gotthard massif (central Swiss Alps)]. Eclogae Geol Helv 83:77–97

Masset O, Loew S (2007) Spatial distribution of tunnel inflows in the Central Aar and Gotthard Massifs (Switzerland). In: Ribeiro L, Chambel A, de Melo MTC (eds) XXXV Congress of the International Association of Hydrogeologists, Groundwater and Ecosystems, Lisbon, Portugal, September 2007

Mazurek M (1993) Geology of the crystalline basement of Northern Switzerland. Nagra Technical Report NTB 93-12, NGRA, Wettingen, Switzerland

Meyer J, Mazurek M, Alexander WR (1989) Petrographic and mineralogical characterization of fault zones AU 96 and AU 126. In: Bradbury MH (ed) Laboratory investigations in support of the migration experiments at the Grimsel test site. Nagra Technical Report NTB 88-23, NGRA, Wettingen, Switzerland

Molinero J, Samper J, Juanes R (2002) Numerical modeling of the transient hydrogeological response produced by tunnel construction in fractured bedrocks. Eng Geol 64:369–386

Mourzenko VV, Thovert J-F, Adler PM (1996) Geometry of simulated fractures. Phys Rev E 53:5606–5626

Mourzenko VV, Thovert J-F, Adler PM (1999) Percolation and conductivity of self-affine fractures. Phys Rev E 59:4265–4284

Ofterdinger US (2001) Ground water flow systems in the Rotondo Granite, Central Alps (Switzerland). PhD Thesis, ETHZ, Switzerland

Rutqvist J, Stephansson O (2003) The role of hydromechanical coupling in fractured rock engineering. Hydrogeol J 11:7–40

Schmid SM, Pfiffner OA, Froitzheim N, Schönborn G, Kissling E (1996) Geophysical-geological transect and tectonic evolution of the Swiss-Italian Alps. Tectonics 15:1036–1064

Schneider TR (1974) Geologie und Geotektonik der Stollen und Schächte im Abschnitt Brienzwiler-Griespass [Geology and geotectonics of galleries and shafts in the Brienzwiler-Griespass section]. Gas-Wasser-Abwasser 54:278–286

Schneider TR (1981) Wasserführung in bestehenden Untertagebauten im Kristallin der Zentralmassive und des Penninikums im Tessin und Misox [Groundwater in existing underground constructions in crystalline rocks of the Central Massifs and Peninic units in Tessin and Misox]. NIB 81-02, Nagra, Wettingen, Switzerland

Steck A (1968a) Die Alpidischen Strukturen in den Zentralen Aaregraniten des westlichen Aarmassivs [The Alpine structures of the granites in the western Aar massif]. Eclogae Geol Helv 61:19–48

Steck A (1968b) Junge Bruchsysteme in den Zentralalpen [Late Alpine faulting in the Central Alps]. Eclogae Geol Helv 61:387–393

Steck A (1984) Structures de déformations tertiaires dans les Alpes Centrales (Transversale Aar-Simplon-Ossola) [Tertiary deformation structures in the Central Alps (Aar-Simplon-Ossola transverse)]. Eclogae Geol Helv 77:55–100

Steck A, Hunziker J (1994) The tertiary structural and thermal evolution of the Central Alps: Compressional and extentional structures in an orogenic belt. Tectonophysics 238:229–254

Stober I (1995) Die Wasserführung des kristallinen Grundgebirges (Groundwater in the crystalline basement). Enke, Stuttgart, Germany

Stober I (1997) Permeabilites and chemical properties of water in crystalline rocks of the Black Forest, Germany. Aquat Geochem 3:43–60

Stober I, Bucher K (1999) Deep groundwater in the crystalline basement of the Black Forest region. Appl Geochem 14:237–254

Stober I, Bucher K (2007) Hydraulic properties of the crystalline basement. Hydrogeol J 15:213–224

Voborny O, Vomvoris S, Wilson S, Resele G, Hürlimann W (1994) Hydrodynamic synthesis and modeling of groundwater flow in crystaline rocks of northern Switzerland. Nagra Technical Report NTB 92-04, Nagra, Wettingen, Switzerland

Wang M, Kulatilake PHSW, Panda BB, Rucker ML (2001) Groundwater resources evaluation case study via discrete fracture flow modeling. Eng Geol 62:267–291

Wyss R (1986) Die Urseren Zone: Lithostratigraphie und Tektonik [The Urseren zone: lithostratigraphy and tectonics]. Eclogae Geol Helv 79:731–767

Zangerl CJ (2003) Analysis of surface subsidence in crystalline rocks above the Gotthard highway tunnel, Switzerland. PhD Thesis, ETHZ, Switzerland

Zangerl C, Loew S, Eberhardt E (2006) Structure, geometry and formation of brittle discontinuities in anisotropic crystalline rocks of the Central Gotthard Massif, Switzerland. Eclogae Geol Helv 99:271–290

Zangerl C, Evans KF, Eberhardt E, Loew S (2008a) Consolidation settlements above deep tunnels in fractured crystalline rock: part 1, investigations above the Gotthard highway tunnel. Int J Rock Mech Min Sci 45:1195–1210

Zangerl C, Eberhardt E, Evans KF, Loew S (2008b) Consolidation settlements above deep tunnels in fractured crystalline rock: part2, numerical analysis of the Gotthard highway tunnel case study. Int J Rock Mech Min Sci 45:1211–1225

Zangerl C, Evans KF, Eberhardt E, Loew S (2008c) Normal stiffness of fractures in granitic rock: a compilation of laboratory and in-situ experiments. Int J Rock Mech Min Sci 45:1500–1507

Zhang L, Franklin JA (1993) Prediction of water flow into rock tunnels: an analytical solution assuming a hydraulic conductivity gradient. Int J Rock Mech Min Sci 30:37–46

Zhao J (1998) Rock mass hydraulic conductivity of the Bukit Timah granite, Singapore. Eng Geol 50:211–216